ASSESSMENT OF GEOTHERMAL POTENTIAL IN PARTS OF BORNO BASIN NORTH-EAST NIGERIA USING AEROMAGNETIC AND AERORADIOMETRIC DATA

BY

SABO, Mohammed Lawal
MTech/SPS/2017/7063

DEPARTMENT OF PHYSICS
FEDERAL UNIVERSITY OF TECHNOLOGY, MINNA

SEPTEMBER, 2021

SSESSMENT OF GEOTHERMAL POTENTIAL IN PART OF BORNO BASIN NORTH-EAST NIGERIA USING AEROMAGNETIC AND AERORADIOMETRIC DATA

BY

SABO, Mohammed Lawal
MTech/SPS/2017/7063

A THESIS SUBMITTED TO THE POST GRADUATE SCHOOL FEDERAL UNIVERSITY OF TECHNOLOGY, MINNA, NIGER STATE, NIGERIA IN PARTIAL FULFILMENT OF THE REQUIREMENTS FOR THE AWARD OF MASTER DEGREE OF TECHNOLOGY IN APPLIED GEOPHYSICS

SEPTEMBER, 2021

ABSTRACT

This research was aimed towards the assessment of geothermal potential part of Borno Basin north-east Nigeria using aeromagnetic and aeroradiometric data. Regional/Residual separation was performed on the total magnetic intensity map using polynomial fitting, and the residual map was divided into nine spectral blocks of which the log of spectral energies were plotted against frequency. Centroid depth and depth to top boundary obtained was used to estimate the Curie point depths, which were further used in computing the geothermal heat flow of the study area reveals that the curie point depth ranges from 9.74 km to 21.68 km with an average value of 15.71 km. The geothermal gradient, vary between 26.75 ^{o}C/km and 59.55 ^{o}C/km. The results shows that the heat flow values of the study area vary between

71.09 mW/m^2 and 150.07 mW/m^2, low values of 65 mW/m^2 to 90 mW/m^2 are located at the Northeastern and Northwestern part of area (Awiam and Bajoga) and higher value of 100 mW/m^2 to 150 mW/m^2 can be located at most part of the southcentral part (Dukku and Bajoga). This shows that the geothermal heat flow varies between 67.41 mWm^{-2} and 150.07 mWm^{-2}. The aeroradiometric data covering the study area was also analysed to estimate the radiogenic heat contribution. The radioactive heat production values vary between 1.25 µW/m^2 and 2.03 µW/m^2 with an average of 1.43 µW/m^2. The estimated heat flow value of 80 mW/m^2 to 100 mW/m^2 obtained around Awiam, Dukku (north/western), and Nafada and Bajoga (Northeastern and southeastern) region of the study area makes the area to be of favourable for geothermal exploration.

TABLE OF CONTENTS

CHAPTER THREE

LIST OF FIGURES

LIST OF TABLES

APPENDICES

CHAPTER ONE

1.0 INTRODUCTION

1.1 Background of the Study

Geophysics is a very powerful and dynamic tool of exploration and consistently used in reconnaissance surveys. There are many geophysical survey methods, which include gravity, magnetic, radiometric, seismic, electrical resistivity etc. Each of the above survey method has a unique operative physical property like density, magnetic susceptibility, radioactivity, propagation or velocity of seismic waves and electrical conductivity of the Earth (Kearey *et al.,* 2002). These methods were used to investigate the subsurface geology of an area of interest. Some of these methods can still be applied by flying the geophysical equipment namely magnetic, electromagnetic, gravity and radiometric. Airborne geophysics is an effective way for surveying a very large area quickly for regional exploration.

The quest for renewable energy sources as a means of alternative energy to carter for the dwindling rate of power supply, which will meet up with the current population growth and industrial development in Nigeria, has necessitated the need for this survey. A high resolution Aeromagnetic and Aeroradiometric data over part of Borno Basin, an extension of the Nigeria part of Chad Basin, has been analysed and interpreted quantitatively with the aim of investigating the study area for possibility of geothermal potentials by estimating the Curie point depth and the heat flow of the study area based on a reconnaissance for geothermal energy.

The Curie point (bottom of magnetic source) is the point within the earth crust at about the temperature of 580 °C where magnetic properties of rocks disappears and magnetic minerals show paramagnetic susceptibility (Khojamli *et al.*, 2016).

Depending on the geology and rock mineral contents, Curie point temperature varies from area to area. It is therefore normal to expect minimum Curie point depth (CPD) at the regions which have geothermal potential, young volcanisms and a thin crust (Aydın and Oksum, 2010). The assessment of the disparities in the CPD of a particular region can give a preliminary and appreciated information about the area temperature distribution at a depth and the geothermal energy potential of the subsurface (Tselentis, 1991).

In some part of Nigeria; Ikogosi in Southwest and Wikki in the North Central, there are geological evidence of warm spring and hot spring respectively, which have signs of good indication for geothermal energy potential. The aeromagnetic and airborne radiometric data of part of Borno Basin based on a reconnaissance survey was used to assess the geothermal energy potentials in the study area.

1.2 Statement of the Research Problem

Presently, there is an inconsistent supply of power in the country, because the hydroelectricity needs constant supply of water and we experience a two-season period (rainy and dry) in Nigeria. During dry season, hydroelectric dams usually have low level of water for our power plant to function well. Household generators are noisy hazardous with high emission of carbon dioxide into the atmosphere.

Other power sources that have been explored are unreliable, very expensive to maintain and in most cases are hazardous to the environment. The availability of geothermal energy which results from radioactive decay of minerals within Earth’s core are readily utilised by several countries of the world. However, in Nigeria quite a little of this energy alternative source is known. This is even with the existence of the known potential entities such as; Ikogosi warm spring (37 ^{0}c) in Ondo State, Wikki warm spring (39 ^{0}c) in Bauchi State and Rafin-Ruwa warm spring (45 ^{0}c) in Plateau State.

1.3 Justification for the Study

Assessing the geothermal potential in Borno basin will help determine areas of good geothermal energy to augment and boost power supply in the study area. In addition, keen interest on the importance and uses of geothermal energy, which is a non-fossil fuel energy source, is very important in the quest to boost Nigeria's current grid. Quite importantly, almost all aspect of human life require energy.

1.4 Aim and Objectives of the Study

The aim of this study is to assess the geothermal potential in part of Borno basin using Aeromagnetic and Aeroradiometric data.

The objectives of the study are to:

i. produce and interpret the composite total magnetic intensity (TMI) map and the ternary concentration maps of the radionuclide elements (Uranium, Thorium and Potassium).

ii. separate the composite (total magnetic intensity) map into regional and residual components.

iii. use spectral analysis to reveal Curie point depth, geothermal gradient and Heat flow.

iv. interpret the radiometric data for possible radiogenic heat contribution.

v. delineate areas suitable for geothermal exploration and exploitation.

CHAPTER TWO

2.0 LITERATURE REVIEW

2.1 Geology of the Study Area

The study area (Figure 2.1) is located within Borno Basin, which represents the Nigeria section of the Chad Basin, it is one of Nigeria's inland basins located in the northeastern part of the country. It represents about one-tenth of the total areal extent of the Chad Basin, which extends to Cameroon, Niger Republic and Chad.

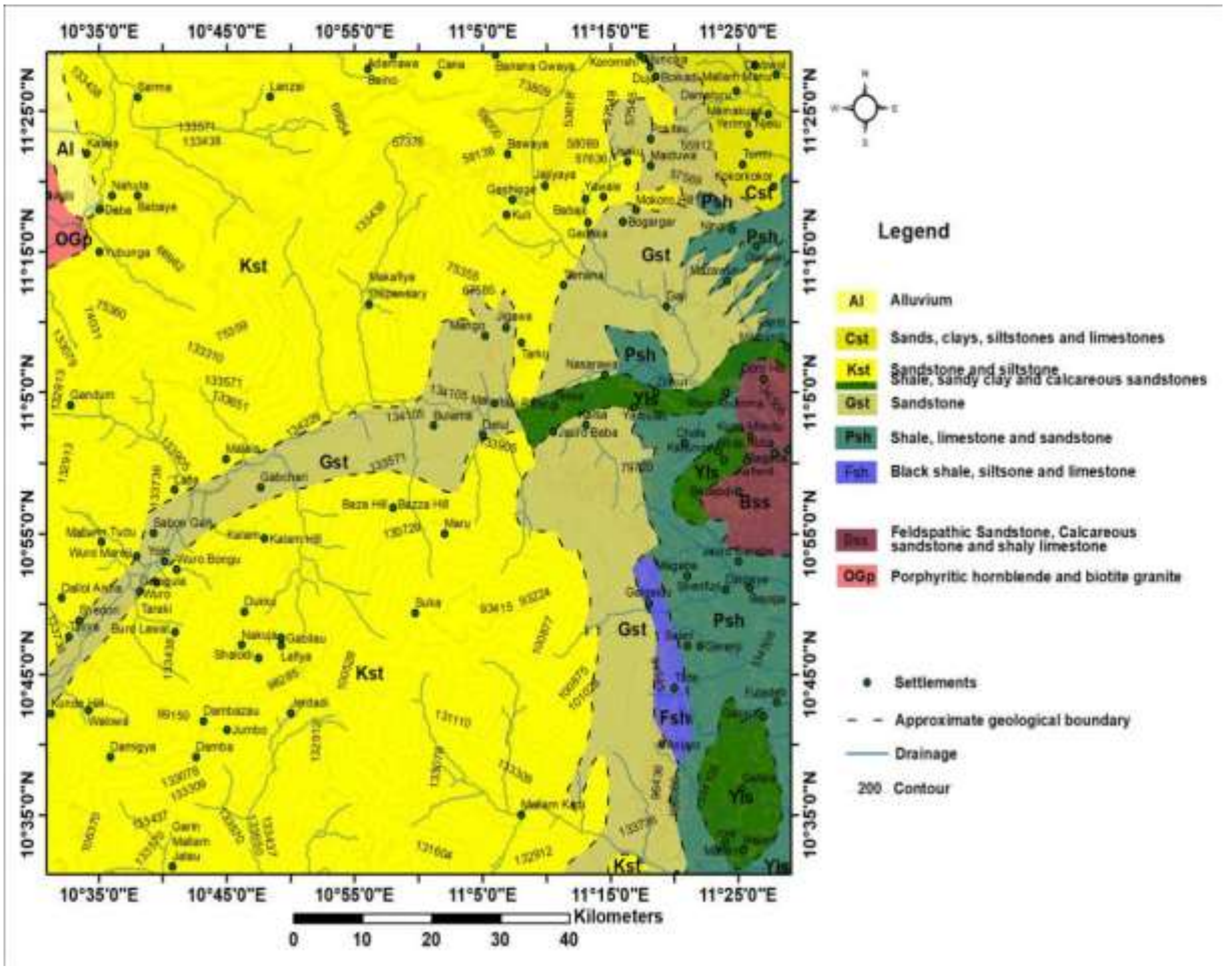

Figure 2.1: Geology Map of the Study Area (Adopted from Obaje, 2009)

2.2 Location of the Study Area

The study area (Figure 1.1 and Figure 1.2) is part of Borno Basin covering Awiam, Nafada, Dukku and Bajoga in the Northeastern part of Nigeria, (Figure 1.1). It is bounded by latitude 10.5^{o} N to 11.5^{o} N and Longitude 10.5^{o} E to 11.5^{o} E. the physiological features recognised in the area is the river Gongola running from the northern part through the eastern part of the study area.

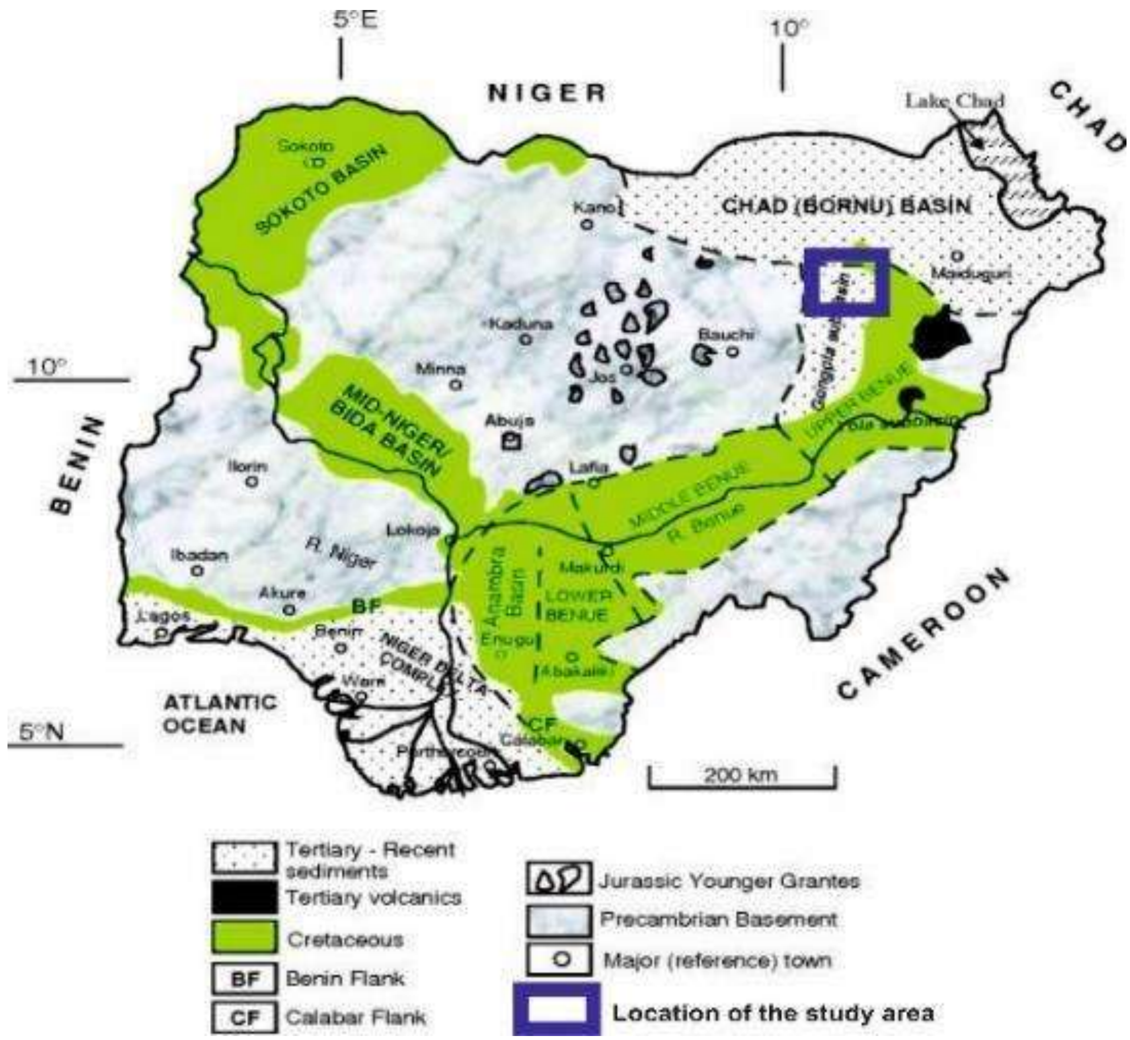

Figure 2.2: Map of Nigeria showing the study area (Obaje, 2009)

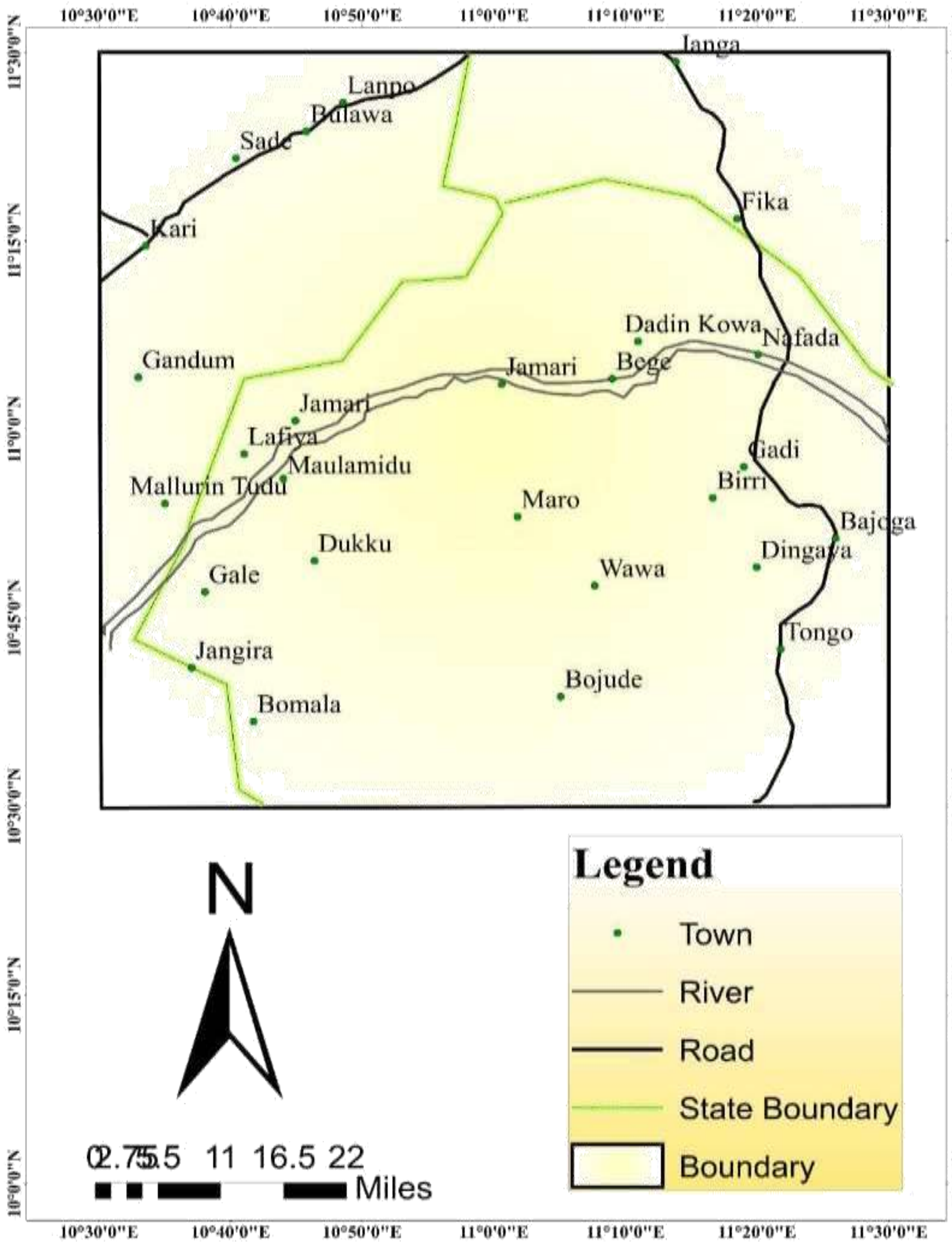

Figure 2.3: Geological map of Nigeria showing location of the study area (Obaje, 2009)

Surveys such as Aeromagnetic and Aeroradiometric are entrenched ways of bringing out signs of lithologic contrast, faults, folds, and concentrations of ore. The radiometric method has extensively been used in many fields. This method was initially used mainly for the exploration of uranium. Lately, it has been employed as a geological mapping tool in mineral exploration.

A comprehensive geologic and geophysical research in Borno Basin and both have led to a detailed insight of the structure, evolution and origin.

Abraham *et al*. (2014) uses aeromagnetic data to estimate the heat flow of part of Ekiti state, they correlate there result with radiogenic heat production (RHP) value obtained from the analysis of aero radiometric'data. He obtained an average value of 91.2 m^2 for the area heat flow and a value of 4.06 m^3 for (RHP). They noted that their RHP was relatively higher when compared to the average heat production of the Precambrian shield, 0.77 to 0.08 m^3. And they attribute this significant increase in RHP value to the high radioelement contents in the area.

Akande *et al*. (2011) carried out a detailed geologic work on Stratigraphic Evolution and Petroleum Potential of Middle Cretaceous Sediments in the Lower and Middle Benue Trough, Nigeria with the aim of expatiating some previously reported source rock data of the Cretaceous formations by detailed mapping of the source rock stratigraphic intervals on the basis of their structural setting, lithologic characteristics, sedimentology and depositional environments. They concluded that In the Middle Benue trough, the preserved iron in the area. They established that most sedimentary rocks of the middle Benue trough were deposited under almost similar geological processes but not at the same time while the dissimilarity observed in the volcanic is due to the fact that they are relatively the youngest as they can be seen to intrude the Late Albian-Cenomanian Awe and Keana Formations.

They also noted that the sandstone are quartz arenites as they were basically of quartz.

Borno basin belongs to Tertiary-Recent sediments (Figure 1.1) and later rift basins in Central and West Africa whose origin is related to the opening of the South Atlantic (Obaje *et al.,* 1998; Genik, 1992).

Nigeria geological survey agency and some mining organisations in their pursuit for locating Uranium and some other mineral deposits in Borno Basin carried out the radiometric estimation and the premise of the sea background of 100 cps to 300 cps have been set up for the Benue trough and Borno Basin with the cretaceous sediments having estimation of between 50 cps to 150 cps. The local occurrence of values of as high as 500 cps to 20000 cps have been explained to indicate the occurrence of rocks rich in Uranium, Potassium and Thorium (Ajakaiye, I981).

According to Adighije, (1979), translated the centra1 regional positive anomaly recorded in shallowing of 10-12 km of the Moho, the consequence of contemporaneous extending and diminishing of the crust under the trough. They registered the depth to the Moho underneath the trough to shift from 22-27 km in the north to 31 - 37km in the south. Their estimate of the rise in Moho, however, is likely too high as a result of the unrealistically little density contrast of 0.17 gcm^3 which they assumed between crust and mantle.

The Chad Basin belongs to the African Phanerozoic sedimentary basins whose origin is related to the dynamic process of plate divergence. Notable exceptions, however, are the deformed sequences of the Paleozoic fold belts of Morocco and Mauritania and the Tindouf and Ougarta basins, which are Paleozoic successor basins. It is an intracratonic inland basin covering a total area of about 2,335,000 km^2 with Niger and Chad Republics sharing more than half of the basin (Burke *et al.,* 1972; Petters, 1977). The area is characterised by a variety of lithological units, which include many types of igneous, metamorphic and sedimentary rocks. The main factors responsible for the sedimentation within the study area are the progressive sea level rise from Albian-Maastrichtian leading to worldwide transgression, regression and local tectonics (Okwesi *et al.,* 2021; Petters, 1978).

2.3 Uses of Geothermal Energy

Geothermal utilisation is commonly divided into two categories; electricity production and direct application for cooking and heating of buildings. Conventional electric power production is commonly limited to fluid temperatures above 180 °C, but considerably lower temperatures can be used with the application of binary fluids (outlet temperatures commonly about 70 °C). The ideal inlet temperatures into buildings for space heating is about 80 °C, but by application of larger radiators in houses/or the application of heat pumps or auxiliary boilers, water with temperatures only a few degrees above the ambient temperature can be used beneficially (Kurowska and Schoeneich, 2010).

2.4 Assessment of Geothermal Energy

Geothermal resource assessment involves studies and research aimed at assessing the nature and energy production capacity of geothermal systems. It is based on the data available at any given time, or stages in the development of a system, such as surface exploration data, the results of the drilling of exploration and production wells.

So far, geothermal assessment has not been widely known in Nigeria, although investigation of subsurface temperature of rock mass was carried out in hundreds wells due to exploration for oil and gas within sedimentary basins. There were several projects aimed at exploration of subsurface temperature distribution, carried out with the use of data from oil and gas boreholes as well as shallow water wells. The results of those studies as well as investigation of geothermal surface manifestations will give an idea about geothermal conditions of Nigeria (Kurowska and Schoeneich, 2010).

2.5 Magnetic Survey

The oldest branch of applied geophysics centered on the study of earth's magnetism. Sir Williams Gilbert (1540 - 1603) made the first scientific investigation of the terrestrial magnetism when he showed that the earth's magnetic field was equivalent to that of a permanent magnet lying in a general North-South direction, near the earth's rotational axis (Telford *et al.,* 1990). The publication of the examination of iron ore deposits by magnetic measurements (Thalen, 1879) marked the beginning of applied geophysics. Since then there have been great advances in instrumentation and interpretation of measurement in the oldest geophysical method of locating both hidden ores and structure associated with deposits of oil and gas.

Magnetic measurement can be carried out on land, in the sea and in the air to find the distribution of magnetized material whose magnetic field is given on a plane surface i.e. measurement of variation in the earth's magnetic field. Local variation introduced by magnetic properties of rock near the surface cause minute (in some cases, large) changes in the main field. These changes are the target of magnetic exploration that map the distribution of magnetic material in the earth's crust. The major magnetic minerals are magnetite, Titan hematite, pyrotite and native iron or Fe-Ni-Co alloys. These minerals give rise to magnetic anomalies, either because of their abnormally large magnetic susceptibilities or because of the high permanent magnetisation (Grant and West, 1965) of the magnetic minerals that occur in nature. Magnetite is the most abundant element. Thus, aeromagnetic surveys, in particular, map the magnetite in the rock below the aircraft, the result or which can be used to assist a program of reconnaissance in geological mapping based on widely-spread grid points, since aeromagnetic anomalies can be employed to delineate geological boundaries between sampling points (Kearey *et al.*, 2002). The magnetic method is very suitable for locating buried magnetic ore bodies because of their high magnetic susceptibilities. In recent years, there has been an increasing recognition of their importance for evaluating prospective area by virtue of the unique information they provide. Sharma (1987) and Udensi (2001) outline the roles of aeromagnetic surveys as follows:

(a) Delineation of volcano, sedimentary belt under sand or other recent covers or in strongly metamorphosed terrain when recent lithologies are otherwise unrecognisable.

(b) Recognition and interpretation of faulting, shearing and fracturing not only as potential host for a variety of minerals, but also as an indirect guide to epigenetic, stress related to mineralisation in the surrounding rocks.

(c) Identification and delineation of post-tectonic intrusion. Typical of such target are zoned syenite or carbonite complexes, Kinerlite, tin bearing granite and mafic-intrusions.

(d) Direct detection of deposits of certain iron Ores

(e) In oil exploration aeromagnetic data can be used to determine the depth to basement beneath the sediment.

However, sedimentary rocks exert such a small magnetic effect compared with igneous rock that virtually all variation in magnetic intensity measurable at the surface result from topographic or lithologic changes associated with the basement or from igneous intrusion.

2.6 Aeromagnetic Survey

Aeromagnetic survey is the common type of airborne geophysical survey and has been recognised as a principal mapping tool for materials that are strongly magnetised (Murthy, 2007). This method seeks to investigate the geology of the particular area due to the differences in the geomagnetic field. These differences are because of the magnetic features of the rocks subsurface (Kearey *et al.,* 2002). The most vital magnetic minerals in soils are the iron oxides, such as magnetite. In soils the main source of magnetic minerals is the parent material through the soil formation processes. A general practice to identify the existence and concentration of magnetic minerals is the amount of the magnetic susceptibility in soils. Soil magnetic susceptibility can be related to different terrain topographic attributes such as the slope, elevation and concavity-convexity of the surface terrain to explain the distribution of magnetic minerals within soils (Quijano *et al.*, 2011)

2.7 Airborne Radiometric Survey

Radiometric method is used in the mapping for radioactive mineral reserves needed for this purpose, and for non-radioactive reserves related with radioactive elements (Kearey *et al.,* 2002). Radiometric data were collected above the ground by flying an airplane with a spectrometer for regional surveys. Gamma rays arising from the decaying of unstable nuclei from the rocks are recorded in the radiometric survey. The entire noticeable gamma radiation from soil minerals occur from the natural breaking down of only three radioactive elements, which are thorium, potassium and uranium. Similarly, the aeromagnetic technique is an effective way of identifying and delineating only magnetite rich minerals within the earth, so as the airborne radiometric technique is efficient in the identification of only the existence of Thorium (Th), Uranium (U) and Potassium (K) at the Earth's surface (Kearey *et al.*, 2002). Due to the depth of penetration, which is, only 30 cm, rocks beneath are inferred from the energies of Uranium, Thorium and Potassium released by the parent rock within a specified region.

Over the last few years, the search for radioactive minerals has turn out to be very important because recent need of nuclear energy fuels. Based on this reason, most of the equipment used for radiometric surveys were manufactured with uranium being the main focus until the new applications were found.

1.8 Source of Data

The aeromagnetic and aeroradiometric datasets for part of Borno basin North East Nigeria were acquired from the Nigeria Geological Survey Agency, Abuja which were collected in 2009. These datasets were processed and the resulting grids and images were interpreted. These grids and images were interpreted in relation to patterns in geology, and the patterns were deduced with regards to known or supposed relationships between rock types, structure, stratigraphic order and ore mineralisation. These patterns helped to delineate and outlined the local geological structures like the shear zones and faults.

2.9 Previous Geophysical Studies

Abraham *et al.* (2014) uses aeromagnetic data to estimate the heat flow of part of Ekiti state, associate the result with radiometric heat production (RHP) value obtained from the analysis of aeroradiometric data. Obtained an average value of 91.2 m^{-2} for the area heat flow and a value of 4.06 m-^{3} for (RHP). Noted that their RHP was relatively higher when compared to the average heat production of the Precambrian shield, 0.77 to 0.08 m^{-3}. And they attribute this significant increase in RHP value to the high radioelement contents in the area.

Muhammed and Mustapha (2014) in order to evaluate magnetic basement depth over parts of Bajoga and environs of part of upper Benue trough estimated the magnetic residual anomaly of high value of +116 nT for Malleri and Dukku portion and low values of about l34nT for Bajoga and Bage portion. Nwosu (2014) used source parameter imaging of aeromagnetic data to estimate depth to Magnetic Basement over Parts of Middle Benue Trough, he established a two-layer depth model and predominant NE-SW lineament trend, his shallower magnetic source (d1) has an average depth of 1079.5 m while the deeper magnetic source bodies (d2) have an average depth of 3245 m.

Abdullah *et al.* (2014) investigate the magnetic exploration of the upper and lower part of the Benue trough for metallic deposits and hydrocarbon. They found the depth to intrusive to range 3.2 km and 3.9 km and depth to deep structure range from 8.7 to 9.2 km. They concluded that most of the intrusive are dyke shape which they suggested that the intrusive might contains Rholerite, Basalt Granite and Dolerite.

Megwara *et al.* (2013) determine the geothermal heat flow and radioactive heat characteristics of the Bida basin using Aeromagnetic and aeroradiometric data covering the area. The research results gave average geothermal heat flow value of 90.959 µW/m^{2} and an average radioactive heat flow value of 2.28 µW/m^{2}.

Salako and Udensi (2013) carried out spectral analysis of part of upper Benue trough in order to established sedimentary thickness beneath the surface in the area. From the result of their study they established two layers with the first layer depth ranges between 0.268 km to l.08 km with maximum depth at the north central part and the minimum depth at south eastern and south western part; they attributed this first layer depth to the magnetic rocks that intrude the sedimentary formation, While the second layer thickness ranges from 2.06 km to3.35 km with highest of 3.35 km attained at the northern part of the area which corresponds to Damaturu and Bulkachuwa area. They attributed the second layer depth to magnetic rocks that are emplaced or intruded into the basement underlying the sedimentary basin. And they finally suggested that the area should be subjected for further geophysical techniques like seismic, reflection and refraction for the purpose of ascertaining the area for hydrocarbon potential.

Kasidi and Nur (2013) estimated Curie depth from spectral analysis of Magnetic data covering Sarti and environs at the North-Eastern Nigeria. The determined curie depth which varies between 26 to 28 km, geothermal gradient varies between 21 and 23 $^{o}Ckm^{-1}$ and the heat flow values 53 to 58 mWm^{-2}.

Eleta and Udensi (2012) estimated the depth to the Curie Point Isotherm of the Eastern sector of Central Nigeria (part of middle Benue Trough) by subjecting the residual data obtained from that area to spectral analysis. Their result show that the Curie point isotherm of the region varies between 2 km and 8.4 km.

Bako (2010) in order to assess the geothermal energy potential in Nassarawa portion of the middle Benue trough using borehole method, considered about 150 boreholes and seven thermal springs (Akiri, Awe 1, Awe 2, Keana, Ribi, Kanje and Azara) he measured the boreholes water temperature at depth and springs temperature, with Akiri spring having the highest recorded temperature of 53 °C. He noted that numerous positive geothermal anomalies were located in the area with peak geothermal gradient of 9.3 ^{O}C/ 100 m around the Awe anticline compare to the general values of about 1.5-2.5 ^{O}C/ 100 m outside the anomalous areas, he further explained that temperatures at higher depths around these anomalous areas will yield greater amount of geothermal energy as geothermal gradient at 100 m equals 9.3 ^{O}C.

Nwogbo (1997) in order to estimate location of magnetic source mapped shallow source in the upper Benue trough using spectral analysis and He established that the mean depth basement varies between 2km to 2.62 km which conforms to the region from topography. Mean depth to the shallow source ranges from 0.07 km to 0.63km which he said may be associated to either shallow intrusive bodies or some close surface basement. He noted that there are few deeper intrusive at 2.45 km within the basement.

Onuoha *et al.* (1994) carried out two-dimensional spectral analysis of Aeromagnetic data over the middle Benue Trough in order to estimates average to magnetic source in the area. Their result indicate two depth source model with depth to deeper source varying between 1.6 km to 5 km while that of shallower source vary in between 0.06 km to 1.2 km.

Ofoegbu and Onuoha (1991) used the 2D spectral analysis of aeromagnetic data to estimate depth to buried magnetic basement over the Abakiliki Anticlinorium part of the lower Benue trough, he established two source model with deeper source depth vary in between 1.2 km to 2.5 km. He reported that the confined linear magnetic components which are conspicuous on the aeromagnetic considered in details affirmed that the anomalies over such magnetic structure (which in various ways has spatial dimension that exceed 10 km) were modeled in terms of dyke like bodies. He established that base on sediment thickness in the region they inferred that the occurrence of various intrusive and deformational history of sediments in Abakiliki Anticlinorium that the region may not have large deposits of hydrocarbon.

CHAPTER THREE

3.0 MATERIALS AND METHOD

3.1 Materials

The materials employed for this study includes the following

i. Aeromagnetic data covering the study area.
ii. Radiometric data covering the study area.
iii. Oasis Montaj Software (version 8.4).
iv. Microsoft Office (Word and Excel Packages).
v. Laptop (work station).
vi. Surfer 15 software.
vii. Matrix Laboratory (Matlab).

3.2 Aeromagnetic Data Acquisition

For this study, four aeromagnetic and aeroradiometric data sheets used were procured from the Nigerian Geological Survey Agency (NGSA) Abuja as part of the nation aeromagnetic and aero-radiometric study carried out in 2009 by Fugro Airborne survey. These four aeromagnetic data sheets used are **108 (Awiam), 109 (Nafada), 130 (Dukku) and 131 (Bajoga)** which correspond to latitude 10^{o} 30′N to 11^{o} 30′N and Longitude 10^{o} 30′E to 11^{o} 30′E. Each scaled/measures 1:100, 000 topographical sheet.

The sheets numbered names of places and coordinates (latitude and longitude) written for easy reference and identification. A correction based on the international geomagnetic reference field (IGRF).

3.3 Data Analysis

The first step in this work is to use the data sheets to produce Total magnetic intensity (TMI) map

i. The next step is to separate regional from the TMI to get the residual.
ii. The residual magnetic data will be subjected to spectral analysis in other to estimate the curie point depth.
iii. The curie point depth will be used to estimate the heat flow.
iv. Both heat flow and curie point depth will be used to assess the possibility of geothermal exploration and exploration in the area.
v. The study area will also be subjected to radiometric analysis for the radiogenic heat contribution.

3.4 Production of Total Magnetic Intensity (TMI) map

The four aeromagnetic sheets were assembled, merged, transported into Oasis montaj 6.42v software to produce the map of the total magnetic intensity (TMI). The Oasis montaj software is primarily designed for potential data analyses, which uses Fourier domain techniques for data transformation.

3.5 Regional and Residual Separation

The Total Magnetic Intensity and even the aeromagnetic field sheet used in the producing it are the entirety of the effect of all sources generating the magnetic anomaly. In applied geophysics, the issue is to dispose with or lessen to a minimum, the impacts of deep seated non-profitable sources with minimum disturbance of the resultant anomaly as could reasonably be expected. A geophysical anomaly is normally made out of a wide range of frequencies, each frequency being defined by particular amplitude. The anomaly of importance might be defined by "noise" comprising of regional patterns, uninteresting geologic variety, and instrument drift. In the event that both anomaly and noise content are known, and there is no overlapping between them, then a channel of concern would be created to wipe out the noise impacts.

Thus, this work (interpretation of the magnetic field) begins with the separation of the long-wavelength anomalies of the regional field component, which is attributed to deep and large scale sources from the shorter wavelength features constituting the residual field assumed to arise from shallow and small scale sources.

3.6 Structural Trend

Lineaments are major topographical features or geological structures usually in linear or curvilinear continuous or discontinuous over an entire length. Lineaments may result from faults, joints, folds, contacts or other geological reasons, and are found in igneous, sedimentary and metamorphic rocks. Lineaments could be a favourable structural condition for the control of mineral deposits in an area (Ananaba and Ajakaiye, 1987; Megwara *et al.*, 2013; Megwara and Udensi, 2014).

3.7 Polynomial Fitting

It is the most flexible of all the analytical methods for separating regional from residual, it includes matching of the regional field with a low order polynomial surface in order to expose the residual elements as random errors. The techniques depend on statistical theory. The regional pattern is represented by a straight line or generally by a smooth polynomial curve.

The observed data are used to process, usually by least square, the mathematical describable surface giving the closest fit to the magnetic field that can be obtained within a specified degree of detail. This surface is considered to be the regional field and the residual field is the difference between the total magnetic field value and the regional field value (Udensi, 2000). This was the method utilized in this work. The method becomes useful because of the limited spatial extent of the study area. It was assumed that the regional field is a first-degree polynomial surface, regional were therefore calculated as two dimensional (2-D) first degree polynomial surface.

A Computer software (Oasis Montaj) was used to derive the residual magnetic valued by subtracting values of the regional field from the total magnetic values at the grid cross point as described above.

3.8 Depth Analysis

The method employed in the analysis of depth are source parameter imaging and spectral analytical method.

3.8.1 The analytical signal amplitude technique

Nabigian (1972 & 1984), was the first to relate the energy of magnetic anomalies to analytical signal. He developed the notion of 2-D analytical signal or energy envelope, of magnetic anomalies. An analytical signal is nothing but a complex number of the type:

$$(,) = + \qquad (3.1)$$

With adequate, real and imaginary parts. Roest *et al.*, (1992), showed that the amplitude (absolute value) of the 3-D analytic signal at location (x, y) can be easily derived from the three orthogonal gradients of the total magnetic field using the expression.

$$|A(x, y)| = \sqrt{(\_\_)^2 + (\_\_)^2 + (\_\_)^2} \qquad (3.2)$$

Where; A (x, y) = amplitude of the analytic signal at (x, y)

M = observed magnetic field at (x, y)

3.8.2 Source parameter imaging (SPI)

Magnetic depth estimation plays an important role in magnetic interpretation. Source parameter imaging (SP1) is a complex analytical signal technique, using not only the magnitude of the analytical signal but also the phase. Interpretation of an anomalous magnetic response involves determining the parameters that characterise the source of the anomaly, depth to the top of the structure is a parameter that is commonly sought and SP1 method is one way of determining this depth estimate.

The SPI method estimates the depth from the local wavenumber of the analytical signal. The analytical signal is defined by Nabighian (1972) as

$$(,) = \frac{(,)}{} - \frac{(,)}{} \qquad (3.3)$$

where $_1(,)$= analytic signal

M (x.z) is the magnitude of the anomalous total field, j is the imaginary number,

z and x are Cartesian coordinates for the vertical direction and the horizontal direction perpendicular to strike, respectively. Nabighian (1972) showed that the horizontal and vertical derivative comprising the real and imaginary parts of the 2D analytical signal is related as follow:

$$\frac{(,)}{} - j \frac{\partial M(x,z)}{\partial z} \qquad (3.4)$$

where denotes a Hilbert transform pair.

The local wave number k1 is defined

$$= \frac{}{} \; ^{-1}[/]$$

(3.5)

Salako (2014) and Nwosu (2014) illustrated that the signatures utilised Hilbert transformation pair stated in (3.4). The Hilbert transform and the vertical derivative operators are linear, so the vertical derivative of (3.4) will give the Hilbert transform pair as

$$\frac{^{2}(\,,\,)}{} - j \frac{\partial^2 M(x,z)}{\partial^2 z} \qquad (3.6)$$

Thus the analytic signal could be define based on second-order derivatives, $A_2(x,z)$,

where

$$(x, z) = \frac{^{2}(\,,\,)}{} - j \frac{\partial^2 M(x,z)}{} \qquad (3.7)$$

This gives rise to a second order local wave number K_2, where

$$\frac{}{} \; ^{-1} \; \frac{2}{} \; ^{2} \; \frac{}{} \qquad (3.8)$$

The first and second – order local wave numbers are used to determine the most appropriate model and depth estimate of any assumption about a model.

3.8.3 Spectral analysis of potential field data

The application of spectral analysis to the interpretation of potential field data: gravity and magnetic fields is now sufficiently well established (Spector and Grant, 1970). The method allows an estimate of depth of an ensemble of magnetized/ or density blocks of varying depth, width, thickness and magnetization. Most of the approaches used involve Fourier Transformation of digitized aeromagnetic / or gravity data to compute the energy (or amplitude) spectrum. This is plotted on a logarithmic scale against frequency. The plot shows straight line segments which decreases in slope with increasing frequency. The slopes of the segments yield estimates of average depths to magnetic/or anomalous density sources (Ofoegbu and Onuoha, 1991).

3.9 Energy spectra and depth to magnetic source

Considering the energy spectra] of the total intensity anomaly over a single rectangular block, the expression for the energy spectrum transcribed in polar co-ordinates is as follows (Spector and Grant, 1970).

If $= (^2 + ^2) = \arctan(/)$ (3.9)

Hence the energy spectrum E (r,) is given by

$(,) = 4 ^2 ^2 ^{-2h} (1 - ^{-2h})^2(,) \quad ^2( ) \quad ^2( )$ (3.10)

Where K is the magnetic moment per unit volume of the rectangular block, a and b are the

Width and length k is the magnetic moment per unit depth.

$(,) = \frac{\sin( )}{} = \frac{\sin( )}{}$ (3.11)

$^2( ) = [^2 + (\cos + \sin)^2]$ (3.12)

$$^{2}(\ ) = [\ ^{2} + (\ \cos\ +\ \sin\ )^{2}] \qquad (3.13)$$

where *1*, m and n are direction cosines of the magnetic moment vector.

In order to analyse aeromagnetic maps, the ground is assumed to consist of a number' of independent ensembles of rectangular, vertical sided parallelepiped and each ensemble is characterized by a joint frequency distribution for the depth h, width a, and length b and depth-extent. Thus, applying this hypothesis, it is assumed that the map of the magnetic field intensity over an area, alter the removal of the main geomagnetic component consist of the superposition of a large number of individual anomalies, most of the them overlapping, which are caused by several ensembles of blocks having various dimensions and magnetizations (Shehu *et al.,* 2004, Negi *et al* 1983, Osazuwa *et al.,* 1981).

The average values of inclination and declination of the magnetic vector will not differ appreciably from the inclination and declination of the geomagnetic field for quite a large number of bodies, Spector and Grant (1970) obtained the expression for the ensemble average of the radial spectrum as

$$\{\ (\ )\} = 4\ ^{2}\ ^{2}\{\ ^{-2h}\ \}[(1 - \ ^{-}\ )^{2}][\ ^{2}(\ )] \qquad (3.14)$$

$$\{\ ^{2}(\ )\} = \frac{1}{}\int <\ (\ ,\ )> \qquad (3.15)$$

The ensemble average depth h enters only into the factor

$$\{\ ^{-2h}\ \} = \frac{^{-2h}\quad h(2\ \Delta h)}{4\ \Delta h} \qquad (3.16)$$

where exp (-2hr) term is the dominating factor in the power spectrum which could be approximates for the depth estimations for magnetic field data (Spector and Grant, 1970). Map spectra] are declining functions of r whose rate of decay is largely dominated by the mean depth of the bodies. If there are two sets of sources, then they can be recognized by marked change in the spectral decay rate. The energy spectrum of the double ensemble will then consist of two parts. The first part relates to the deeper sources and it is relatively strong and at low frequencies and hence decays away very quickly. The second part arises from the shallower ensemble of sources, dominates the high frequency end of the spectrum. The radial spectrum could be approximated by straight line segments, the slopes of which relates to the possible layers (Udensi and Osazuwa, 2003; Spector and Grant, 1970).

The residual total magnetic field intensity values are used to obtained the two dimensional Fourier Transform from which the spectrum is to be extracted from the residual values. T(x,y) consisting of M rows and N columns in the x-y plane the two dimensional Fourier Transform is obtained. The evaluation is done using an algorithm that is a two dimensional extension of the fast Fourier Transform (Negi *et al.,* 1983). The frequency intervals Tare subdivided into sub-intervals which lie within one unit of frequency range. The average spectrum of the partial waves falling within this frequency is calculated and the resulting values together constitute the radial spectrum of the analogous field (Udensi and Osazuwa, 2003).

The logarithm of energy values is hence plotted against frequency on a linear scale and the linear segments located. If Z is the mean depth of a layer, the depth factor for this ensemble of anomalies is exp (-2zk). Thus the logarithmic plot of the radial spectrum would give a straight line whose slope is (-2z). The mean depth of burial of the ensemble is thus given as:

$$z = - \frac{\quad}{2} \qquad (3.17)$$

where M is the slope of the best fitting straight line and it is applied directed if the frequency unit is in radians per kilometre. If the unit is in cycles per kilometre, the corresponding relation can be expressed as

$$z = - \frac{}{} \qquad (3.18)$$

3.10 Curie-Point Depth

The centroid depth is calculated from the low watIe number part of the scaled power spectrum as;

$$\ln[\, P(k)^{1/2} / k] = A - k\, Z_o \qquad (3.19)$$

where ln is the natural logarithm, P (k) is the radially averaged power spectrum, k is the Wave number (27t/km). A is a constant depending on the properties magnetization and its orientation and Z_0 is the centroid depth of the magnetic sources (Tanaka *et al.*, 1999).

For the high wave number part, the lower spectrum can be related to the top of the magnetic sources by a similar equation:

$$\ln [P(k)^{1/2}/k] = B - k\, Z_0 \qquad (3.20)$$

where B is a constant: Z_1 is the depth to the top of the magnetic sources. The depth of the bottom of magnetization Z_b is:

$$Z_b = 2Z_0 - Z_t \qquad (3.21)$$

Summarily, the depth to the base of the magnetic source (the Curie point depth) is calculated in four steps (Tanaka *et al.*, 1999):

i. Calculate the radially averaged power spectrum of the magnetic data in each window

ii. Estimate the depth to the top of the magnetic source (Z_t) using the high wave number portion of the magnetic anomaly power spectra

iii. Estimate the depth to the centroid of the magnetic source (Z_0) using a lower wave number portion of the magnetic anomaly power spectra

iv. Calculate the depth to the base of the magnetic source (Z_b) using $Z_b = 2Z_0 - Z_t$.

The value of the Z_b is the Curie point depth.

3.11 Geothermal Gradient

The geothermal gradient in relation to the heat flow q (Tanaka *et al.*, 1999):

q = — (3.22)

The surface temperature is θ°C and — will remain constant provided there are no heat sources or heat sinks between the earth's surface and the Curie point depth. The Curie temperature depends on magnetic mineralogy. For example, although the Curie temperature of magnetite (Fe_3O_4) is at approximately 580°C, an increase of Titanium (Ti) contents of titanomagnetite ($Fe_{2-x}Ti_xO_3$) will cause a reduction of the Cutie temperature. A curie temperature of 580°C and thermal conductivity for igneous rocks will be used in the study as standard (Nwankwo *et al.*, 2011; Tanaka *et al.*, 1999), the author then calculated the value for K the geothermal gradient in the study area using the empirical relation between Curie point, Curie temperature and geothermal gradient (equation 3.22).

3.12 Heat flow

Heat flow estimates on the crust may therefore be made using the depth and thickness information. The Curie point temperature at which rocks lose their ferromagnetic properties provides a link between thermal models and models based on the analysis of magnetic sources.

The magnetic susceptibility and strength of the material that make up the crust are controlled by the temperature. At temperature higher than the Curie point, magnetic ordering is loose and both induced and remnant magnetisation disappear, while for temperatures greater than 580°C those materials will begin to experience ductile deformation. The basic relation for conductive heat transport is Fourier's law. In one dimensional case under assumption that the direction of the temperature variation is vertical and the temperature gradient — is constant; Fourier's law takes the form:

$$= - \quad — \qquad (3.23)$$

Where q is heat flow and k is thermal conductivity. The Curie temperature °C can also be defined as:

$$°C=(\quad —) \qquad (3.24)$$

Where d is the Curie point depth (as obtained from the spectral magnetic anomaly)

3.13 Airborne Radiometric Method

There is appreciation in Geophysical survey when two or more geophysical method are employed. Qualitative analysis of radiometric data over part of the study area with high heat flow and geothermal gradients was undertaken to correlate the complement the result obtained from the analysis of Aeromagnetic data. As most of the continental heat flow emanates from the decay of radioactive isotopes in the crust, therefore locating regions having higher concentration of radioactive isotope or estimating the radioactive heat production can be the same as locating areas with high heat flow (Holmber *et al.*, 2012).

Generally airborne radiometric survey which includes the repeated radiometric measurement of gamma ray flux that strikes at least one detector mounted in a moving grid like pattern aircraft, is always flown in conjunction with the magnetic method. Correction for variation in altitude, atmospheric radon and cosmic radiation are made on the data, the data is then processed to produce results which are expressed as concentration of ^{232}Th, ^{238}U and ^{40}K.

This is based on calibration data collected over sources of known concentration of ^{232}Th, ^{238}U and ^{40}K and test flights over areas of known ground concentrations and radiation level. In this process, two assumptions are made;

i. That the thorium and uranium decay series are in secular equilibrium (i.e activity measurements are made using ^{208}TI in the ^{232}Th decay series and ^{214}BI in the ^{238}U decay series).
ii. The source on the ground are effectively of infinite extent and homogeneous.

3.13.1 Basic principles of radiometric survey

Soils and rocks are radioactive naturally, comprising different degrees of variety of elements showing natural decay and releasing different variety of radiations (alpha, beta and gamma) within a particular energy levels. At present only the gamma ray radiation has adequate energy usable in geophysical mapping or exploration, as it is the only one that is emitted as an electromagnetic wave (Livia *et al.,* 2017), enabling it to be more penetrable compared with alpha and beta, being able to cross bodies and buildings. A gamma spectrum measured in nature therefore yields information about exact concentration of radioactive nuclides in the material detected by the detector system.

Gamma rays usually come in form of very high frequency, resulting in high-energy electromagnetic waves that are spontaneously emitted by the nuclei of some isotopes of some elements. They have comparatively shorter wavelengths and consequently penetrate deeply. Most of the equipment used in recording gamma radiation contain some sort of scintillation crystal setup attached to a variety of multi-channel analysers to translate incoming radiation into flashes of light having intensity proportional to the energy of the absorbed gamma photon.

Natural sources of gamma rays on Earth include consist of decay from few naturally occurring radioisotopes; and among these, there are just three which are common enough within earth materials to make them geologically useful (for differentiating lithologies and soils by their characteristic radioactivity-emissive signatures). These three are K^{40}, U^{238} and Th^{232}. Uranium and Thorium cannot be measured directly. Daughter nuclides (B_i^{214} and TI^{208}) generated during the decay of parent elements (Uranium and Thorium) are measured rather than the abundance of parent elements are inferred. Therefore, Uranium and Thorium are expressed in equivalent parts per million (eU and eTh). B_i^{214} originates from the decay of U^{238} and is consequently, an indicator of uranium concentration in the earth materials that exist within the range of the detector, TI^{208} originates from the decay of Th^{232} and is an indicator of thorium content; and ^{40}K is one of the minor natural isotopes of potassium and the main isotope of potassium that is radioactive (Gupta, 1991).

Gamma rays are defined by their energies, measured in electron volts (eV). The collection of gamma ray has an energy bank known as energy window (Table 3.1), which shows varies from 0.41 to 2.18 MeV within this band; each element represents a channel in the Gamma-ray spectrometer. Potassium isotope is associated with a peak of 1.46 MeV. The isotopes ^{232}Th and ^{238}U, as they do not emit gamma radiations directly, are analysed by their respective radiation decay, since the products (^{208}Th and ^{214}Bi) emit gamma radiation centered on 2.61 and 1.76 MeV, respectively (Livia *et al.*, 2017). One eV is the kinetic energy required by a unit electron in falling through an electrical potential difference of one volt.

Table 3.1: Values of channels and the peaks (in MeV) associated with channels of radiometric elements

Channel	Energy range (MeV)	Peak (MeV)
^{40}K	1.37-1.57	1.46
^{238}U	1.66-1,86	1.76
^{232}K	2.41-2.81	2.61

3.13.2 Natural radioactivity of rocks

The uranium and thorium in igneous rocks are concentrated much in a few accessory minerals such as zircon, sphene and apitite (Slagstad, 2008). Other notably radioactive minerals, such as pyrochlore, thorite, monazite, uraninite, and allanite, are prevalent in nature but are negligible constituents of rocks, and are spread unevenly. The minerals that transmit thorium and uranium are commonly associated with felsic intrusions specifically with younger intrusions; they can be found substantially less in mafic rocks or in volcanics. The uranium and thorium content of rocks usually increases with acidity, with the maximum concentrations located in pegmatites (Slagstad, 2008). The highest concentrations of uranium and thorium in sedimentary rocks are generally found in shales.

For Potassium is predominantly concentrated in feldspars and micas; rocks with none of these minerals have very low potassium. Therefore, mafic and ultramafic rocks has a very low potassium content. The potassium substance of sedimentary rocks is highly variable however it tends to be higher in shale than in carbonates or sandstones.

3.14 Radiometric Data Processing

The gamma radiation registered by the gamma-ray spectrometer in airborne radiometric Survey is composed of the contributions from soil (Terrestrial radiation), atmosphere, aircraft (Background radiation) and cosmic radiation. The aim of airborne radiometric measurements is to measure the radionuclide content of ground using the information of the direct terrestrial gamma radiation. All other contributions are considered as noise and have to be removed. Terrestrial radiation is mostly produced by the decay of the three natural radio isotopes ^{232}Th, ^{238}U and ^{40}K.

Background changes in the level of activity due to “pockets” of radon gas (that originate from Uranium decay) which has gathered in valleys or due to variations in soil moisture content are most times serious problems. These residual levelling problems that may stay behind even after applying background correction can cause artificial lineation or corrugations in contour or colour maps of the data. The application of micro-levelling technique removes or reduces (to the minimum level) this problem from the data. Micro levelling was applied to the data by the Nigeria Geologic Survey Agency to remove corrugations.

As radioactive decay is a random process smoothing was done on the data to get rid of the noise, and the accuracy of all the estimation was governed by statistical laws. The profiles of counting rates are noisy and contouring cannot be done on the data until they have been smoothened.

3.15 Ratio Radioelement Maps and Analysis

Separate radiometric data, radiometric profiles or radiometric contour maps are the output of airborne and ground uranium exploration. However, the general approach for interpreting gamma-ray data is to create a plot display of the three parameter (radiometric contour maps) for the three elements eU, eTh and K. Gamma ray ternary maps reflect the geochemical variations of K, U and Th in the upper 30 cm of the earth's surface (Megwara *et al.,* 2013). It is a composite image that gives a synchronous array of up to three elements on one map. The composite map is produced by altering the red, green and blue phosphors of the display device or yellow, magenta and cyan dyes of a printer in extent to the radioelement measures of the K, Th, U and TC grids. The adoption of red, green and blue for K, Th and U, respectively, is standard for displaying gamma ray spectrometric data. (Slagstad 2008; Megwara *et al.,* 2013).

The following combinations were initiated by the United State GeoIogical Survey (USGS) (Duval, 1983):

i. The potassium composite image consists of the data of K (in red), with the ratios K/eTh (in green) and K/eU (in blue).
ii. The thorium composite image comprises the data of eTh (in red), with the ratios eTh/eU (in green), and eTh/K (in blue).
iii. The uranium composite image comprises of the data of eU (in red) with the ratios eU/eTh (in green) and eU/K (in blue).
iv. The radioelement composite image consists of the data of K (in red), eTh (in green), and eU (in blue).

U, K and Th exist in large content in granitic soil where clay layers are exposed at the surface (yellow, pink and white). Brightest blue/green (highest amounts of U and Th) symbolize exposed ironstone gravel (low potassium level) and these colours become dim with the increase of deep overlying quartz sand. Similarly lower content of U and Th signals can come from soil produced in very weathered (K deficient) substrate. Deep yellow and grey sands of the sandplain appear as brown to black while deep granitic sands (fresh soil) with considerable amounts of potassium feldspars appear as dark red (Livia *et al.*, 2017).

CHAPTER FOUR

4.0 RESULTS AND DISCUSSION

4.1 Qualitative Analysis

The qualitative interpretation of a magnetic anomaly usually begins with a visual inspection of the shape and trends of the major anomalies followed by delineation of the structural trends. A closer examination of the characteristic features of each individual anomaly is then carried out.

4.1.1 Total magnetic intensity (TMI)

Figure 4.1 the total magnetic intensity (TMI) map of the study area covering Nafada and its environs. The northern part of the area could be seen to be dominated with low magnetic intensity, very low magnetic intensity are more to the northwestern part of the area. The southern part of the study area is greatly characterised with high magnetic intensity. This high magnetic intensity are located at Bajoga and Dokku more pronounced in the south part of the TMI map showing that the high magnetic signature trends southeast southwest.

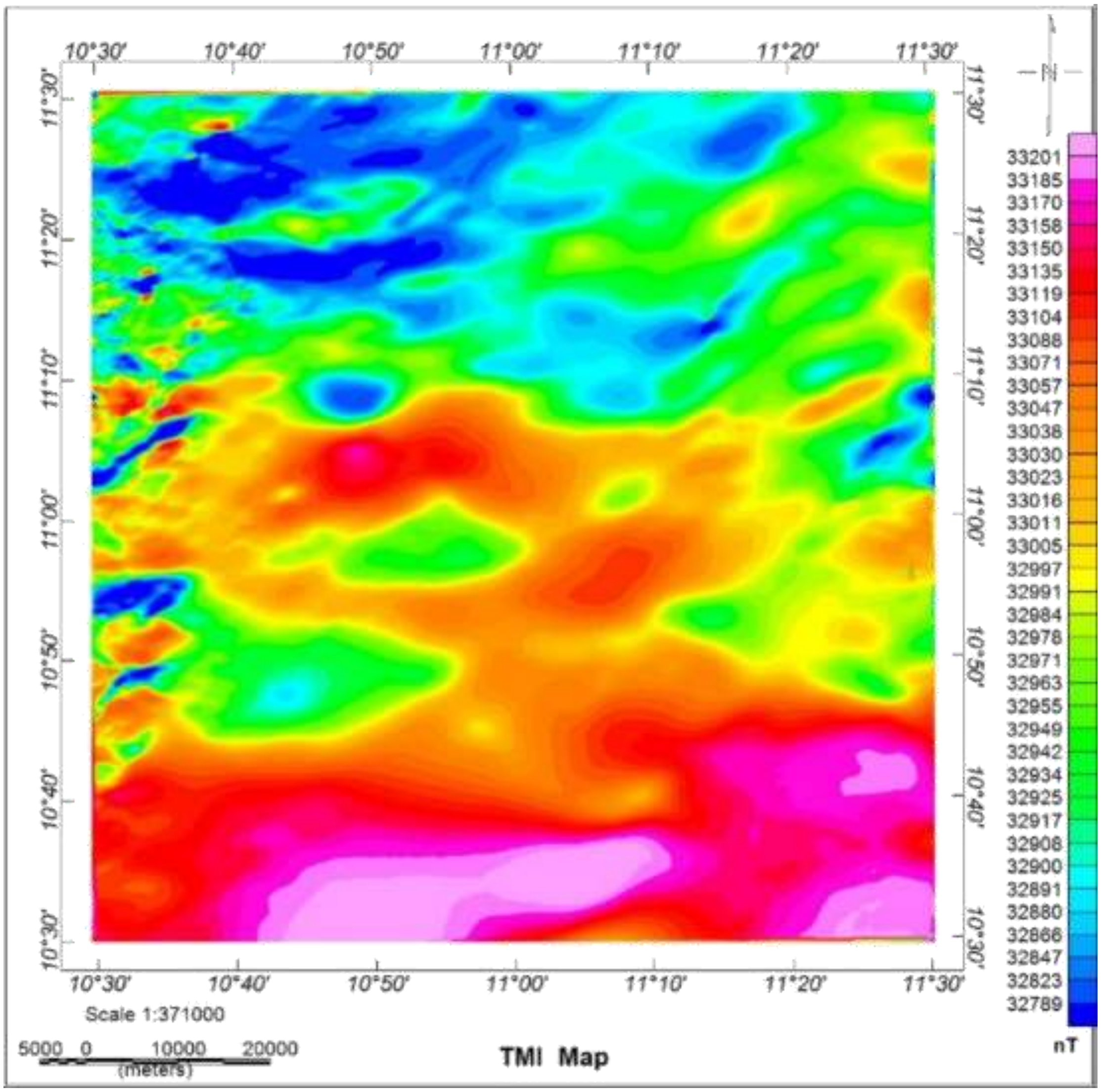

Figure 4.1: Total Magnetic Intensity (TMI) Map of the Study Area

4.1.2 Regional map of the area

The regional map (Figure 4.2) of the study area revealed that the north eastern part of the map is dominated with low magnetic values and high magnetic values are predominant at the south western part of the study area. The regional field generally trends Northwest-Southeast.

The trends appeared in uniform variation (represented by parallel evenly spaced contours) can be observed to run in the NW-SE direction.

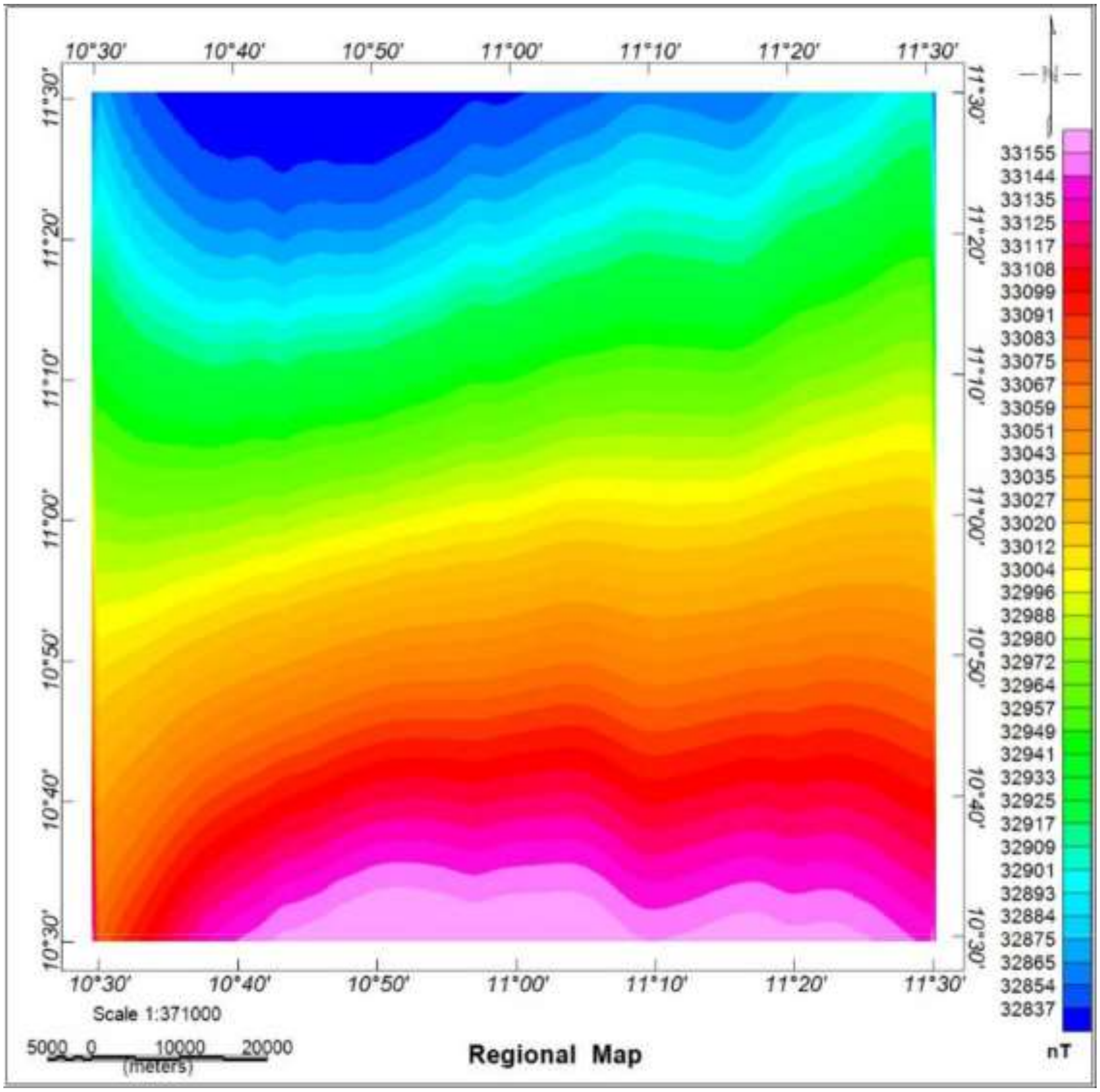

Figure 4.2: Regional Map of the Study Area

4.1.3 Residual map of the area

The residual map (Figure 4.3) of the study area shows that the magnetic intensity values ranges from -130.0 nT to 105.0 nT. The high magnetic anomaly signatures are majorly observed in the north-eastern, south-eastern and southwestern part of the study area. Although, scattered traces are also observed in the northwest and the central parts of the study area.

The low magnetic anomaly signatures can be observed in the west and some minor anomalies are observed scattered elsewhere in the northern, eastern and southern parts of the study area.

The high magnetic anomalies might be as a result of basement intrusion into the sediments while low magnetic anomalies are associated with the sedimentary region.

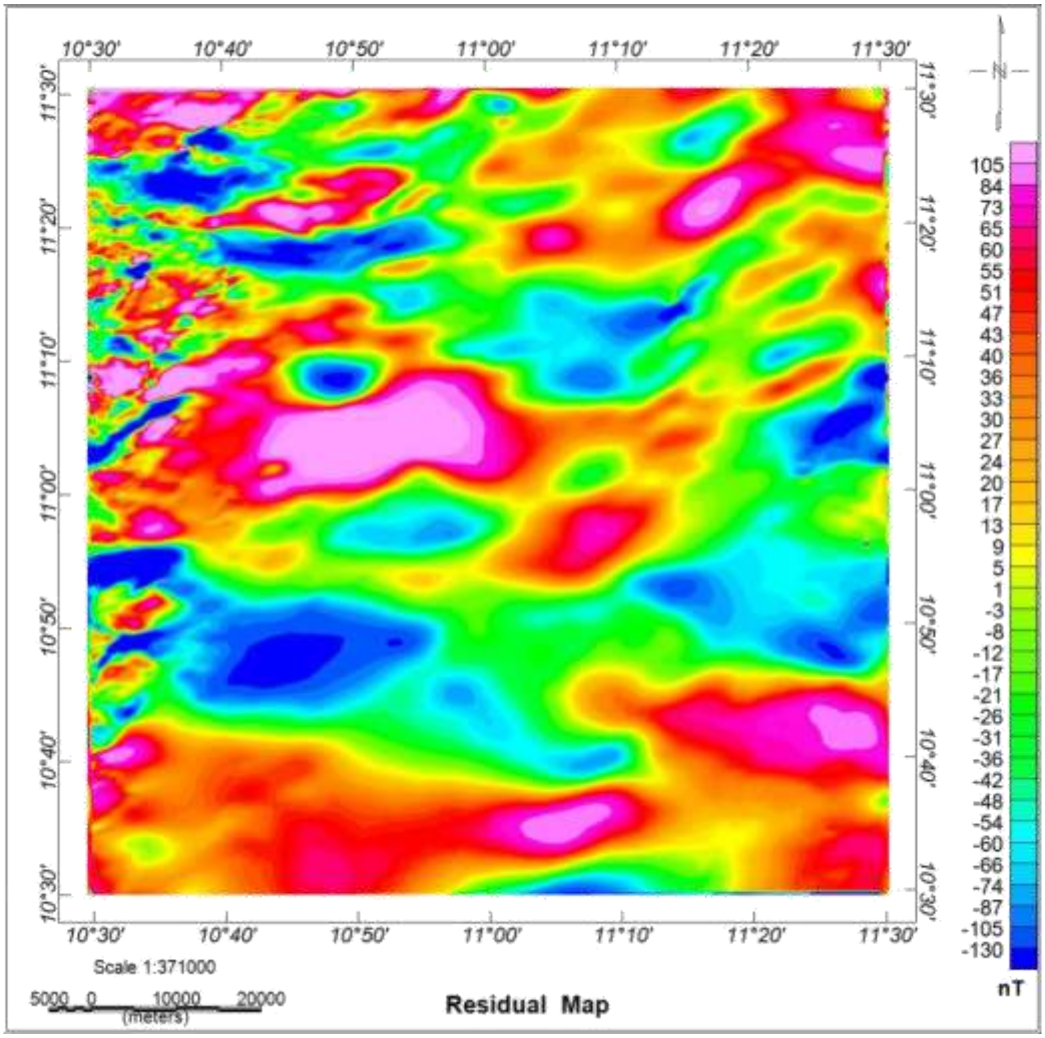

Figure 4.3: Residual Map of the Study Area

4.1.4 Analytic signal

The analytic signal map (Figure 4.4) of the study area disclosed the variation in the amplitude of the magnetic anomalies. The high amplitude values of the analytical signal are prominently observed in the north and western part of the map.

Low amplitude analytic signals are dominantly observed in the central part from the north towards the south-eastern and south-western part of the map. These variations observed conform to the areas of high and low signatures on the residual map (Figure 4.3).

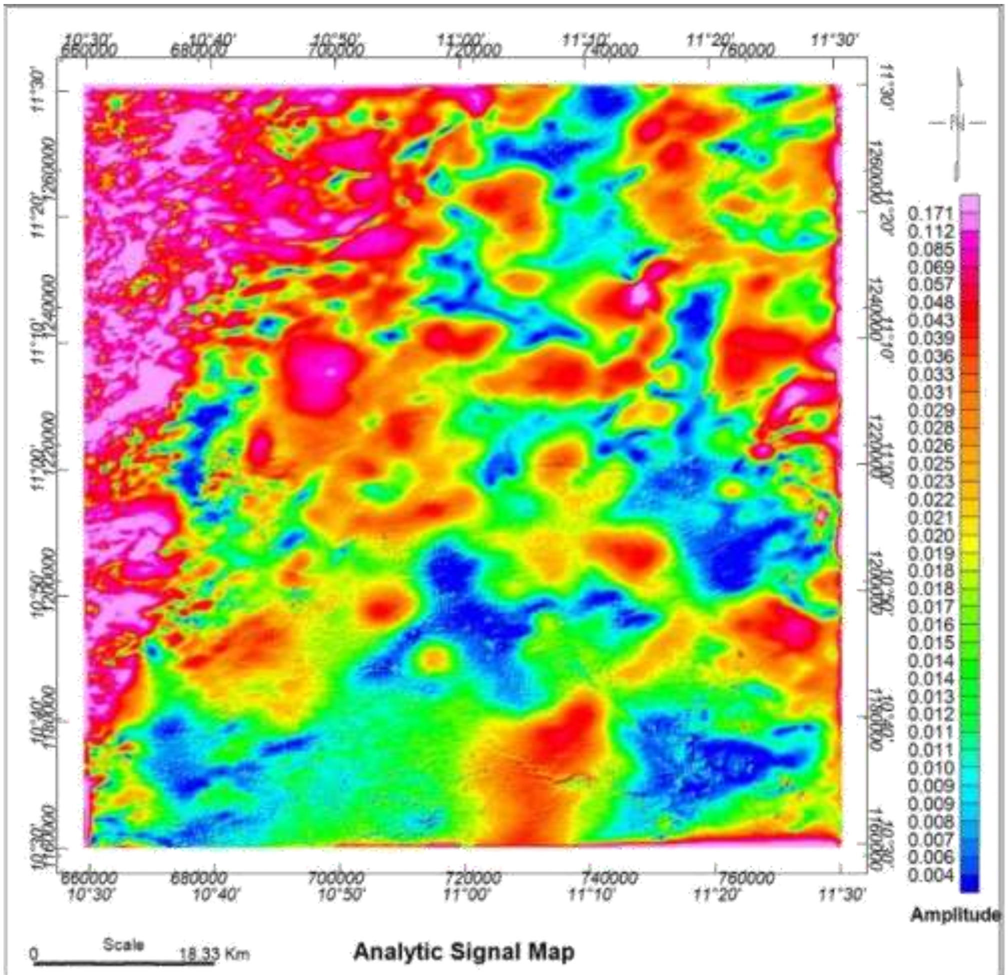

Figure 4.4: Analytic Signal Map of the Study Area

4.2 Quantitative Analysis

In a study exploring sedimentary basin, the assumption is generally made that intrusive rocks within the basement are truncated by erosion at their surface, in this case the depth to the top is equal to the thickness of the sedimentary section. The intrusive may not be extended upward as the basement surface, therefore, any computed sedimentary thickness is generally considered to be minimum.

The depth to the top of the source is a useful tool for finding thickness-of the sedimentary succession and sometimes for locating major structures in basement rocks. Anomalies which arose from basement rocks may be due to lithological changes rather than to structural features. Trend analysis is deducted from magnetic contours which may be drawn out along the fractures or individual anomalies which may be aligned in relation to the fracture system.

An observed magnetic pattern represented on magnetic contour map is the reflection of the contrast between the magnetic properties of the rocks and the observed structural pattern where the trends and intensities of magnetic anomalies are shown on the aeromagnetic map. The dimensions, shape, depth and mass of an anomalous objects are determined from the observed magnetic anomalies. The data obtained are understandably, only approximate, because we are deriving several unknown quantities.

4.2.1 Spectral analyses

The Residual map (Figure 4.3) of the study area was divided into nine (Blocks A - I) overlapping magnetic sections. The division of residual map into spectral sections or blocks were done with Oasis Montaj software. The analysis was carried out using a spectral program plot (SPP) developed with Matrix Laboratory (MATLAB). The graph (Figure 4.5) of the logarithms of the spectral energies against frequencies obtained for block A while other blocks are shown in the Appendices. From the slope of the graph the estimated value for centroid depth and sedimentary thickness were computed (Table 4.1).

The slope of the lower-wave-number part of the wave-number-scaled spectra, which leads to the estimation of centroid depth (Z_0), while the second graph shows the slope of the high-wave-number portion of the spectra, which leads to the estimation of the depth to the top of magnetic sources (Z_t).

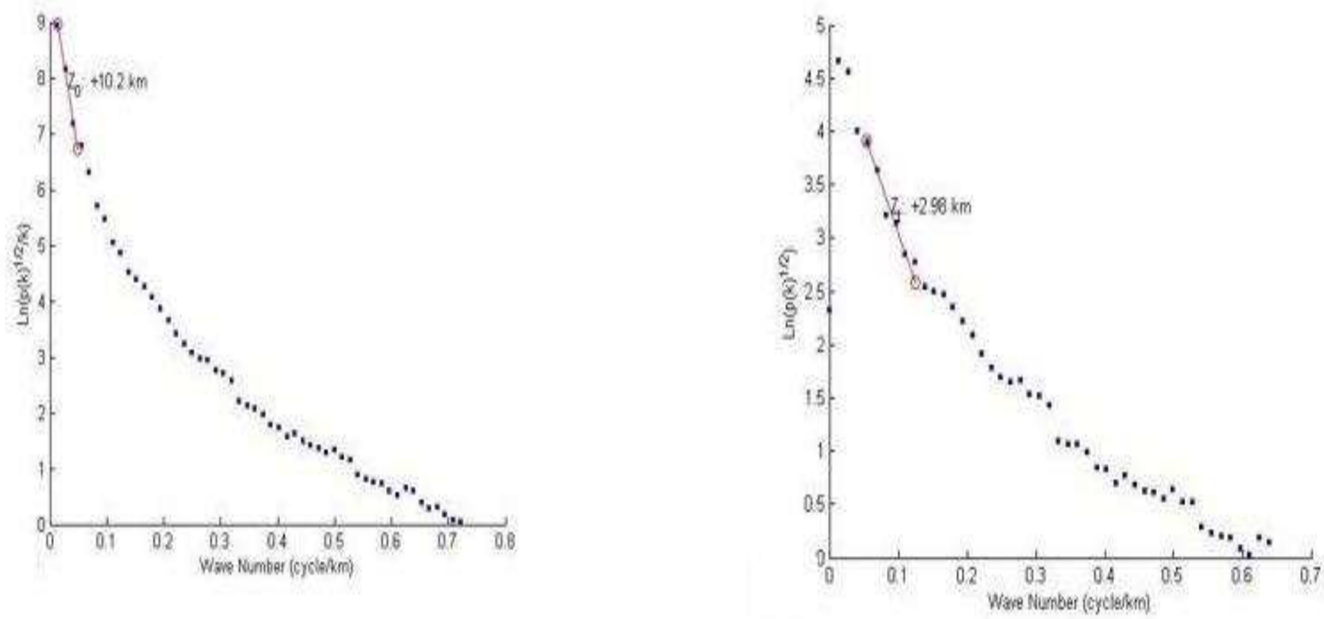

Figure 4.5: Plots of energy against frequency for block A for the determination of Z_0 and Z_t

Table 4.1: Estimated curie point depth, geothermal gradients and heat flow depth for the 9 blocks in the study area

Block	Longitude (Deg.)	Latitude (Deg.)	Zt (km)	Zo (km)	Curie Point Depth (km)	Geothermal gradient ($^oC/km$)	Heat flow (mW/m^2)
A	$10^o30'$-$11^o00'$	$11^o00'$-$11^o30'$	2.98	10.2	17.42	33.30	83.92
B	$11^o00'$-$11^o30'$	$11^o00'$-$11^o30'$	2.95	6.71	10.47	55.40	139.61
C	$10^o30'$-$11^o00'$	$10^o30'$-$11^o00'$	4.14	7.79	11.47	50.70	127.77
D	$11^o00'$-$11^o30'$	$10^o30'$-$11^o00'$	3.94	6.84	9.74	59.55	150.07
E	$10^o30'$-$11^o00'$	$10^o30'$-$11^o30'$	3.31	10.3	17.29	33.55	84.55
F	$11^o00'$-$11^o30'$	$10^o30'$-$11^o30'$	4.12	12.9	21.68	26.75	67.41
G	$10^o30'$-$11^o30'$	$11^o00'$-$11^o30'$	2.92	9.99	17.06	34.00	85.68
H	$10^o30'$-$11^o30'$	$10^o30'$-$11^o00'$	2.84	10.2	17.56	33.03	83.24
I	$10^o30'$-$11^o30'$	$10^o30'$-$11^o30'$	2.24	11.4	20.56	28.21	71.09

The contour map (Figure 4.6) of the depths from the top to the basement (Z_t) reveals the regions of low and high sedimentary thickness. The region of low sedimentary thickness corresponds to the blue colouration in the eastern up to northeastern part while that of the high sedimentary thickness is depicted by the orange colouration in the north and south-western part of the map. The sedimentary thickness ranges between 3.6 km and 4.2 km (found largely between Awiam and Dukku areas).

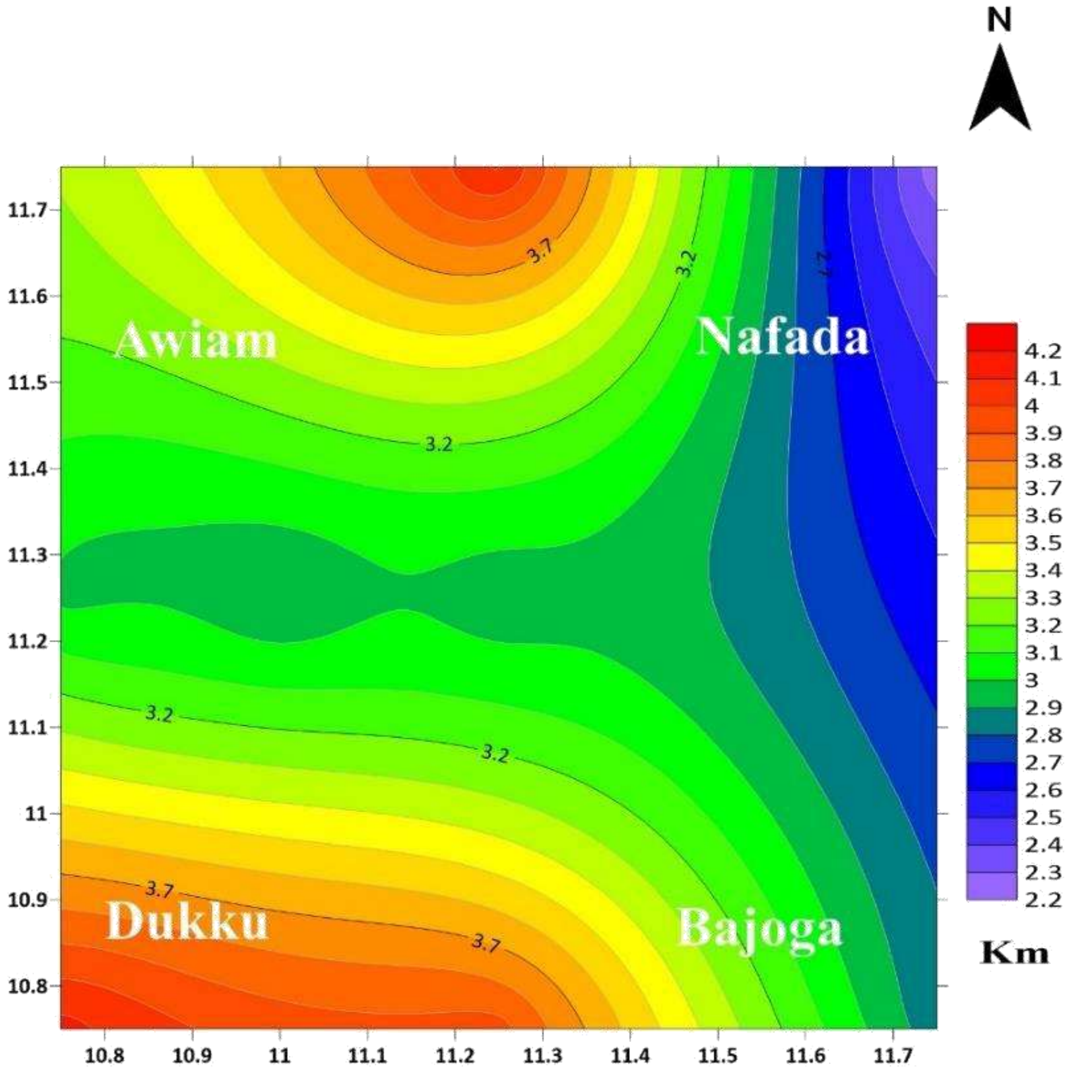

Figure 4.6: Contour map of the depth to top boundary (contour interval is 0.1km)

The depth to centroid (Z_0) and depth of magnetic boundary was used as an input parameter to determine the bottom depth of magnetic bodies Curie Point Depth using equation 2.21, 2.22 and 2.23 are results shown in Table 4.1 reveals that the Curie Point Depth ranges from 9.74 km to 21.68 km with an average value of 15.71km. The Curie Point Depth is deeper at the centre of the western and eastern part of the study area which correspond to part of Awiam and Nafada, and towards part of Bajoga respectively; and shallow at the southern and southwestern part of the study area agree to part of Dukku, respectively.

The Curie temperature approximately 580^{o}C was divided by the estimated Curie Point Depth to give the geothermal gradients for the nine blocks which range from 26.75 $^{o}Ckm^{-1}$ at the top of the northern region of the area to 59.55 $^{o}Ckm^{-1}$ at the lower southern region of the study area with average of 43.88.98 $^{o}Ckm^{-1}$. Table 4.1 gives the heat flow to range from 67.41 mWm^{-1} to 150.10 mWm^{-1} with an average value of 108.76 mWm^{-2}. The heat flow (Figure 4.9) was estimated by multiplying the geothermal gradient by coefficient of thermal gradient of 2.52$Wm^{-1}C^{-1}$. The CPD (Figure 4.7), geothermal gradient (Figure 4.8) and heat flow (Figure 4.9) estimated from this present study agrees with Nwankwo (2011) and Shehu (2004).

The CPD intensely differs according to the geological situations (Ross *et al.,* 2006). The CPDs at volcanic and geothermal areas are shallower than 10 km (Obande *et al.,* 2014). Jessop *et al.* (1976) explained that heat flow of about 80–100 mW/m^2 indicates geothermal anomalous conditions. Objectively, measurement of heat flow determines the quantity of heat energy being vanished. High heat loss anomalies usually concur with the structural trend or areas with thermal manifestations. In this present study, it can therefore be inferred that some part of the study area such as; the southeastern, southwestern, and the central part of the study area are good indicator of geothermal energy potential with shallow CPD, high geothermal gradient and heat flow.

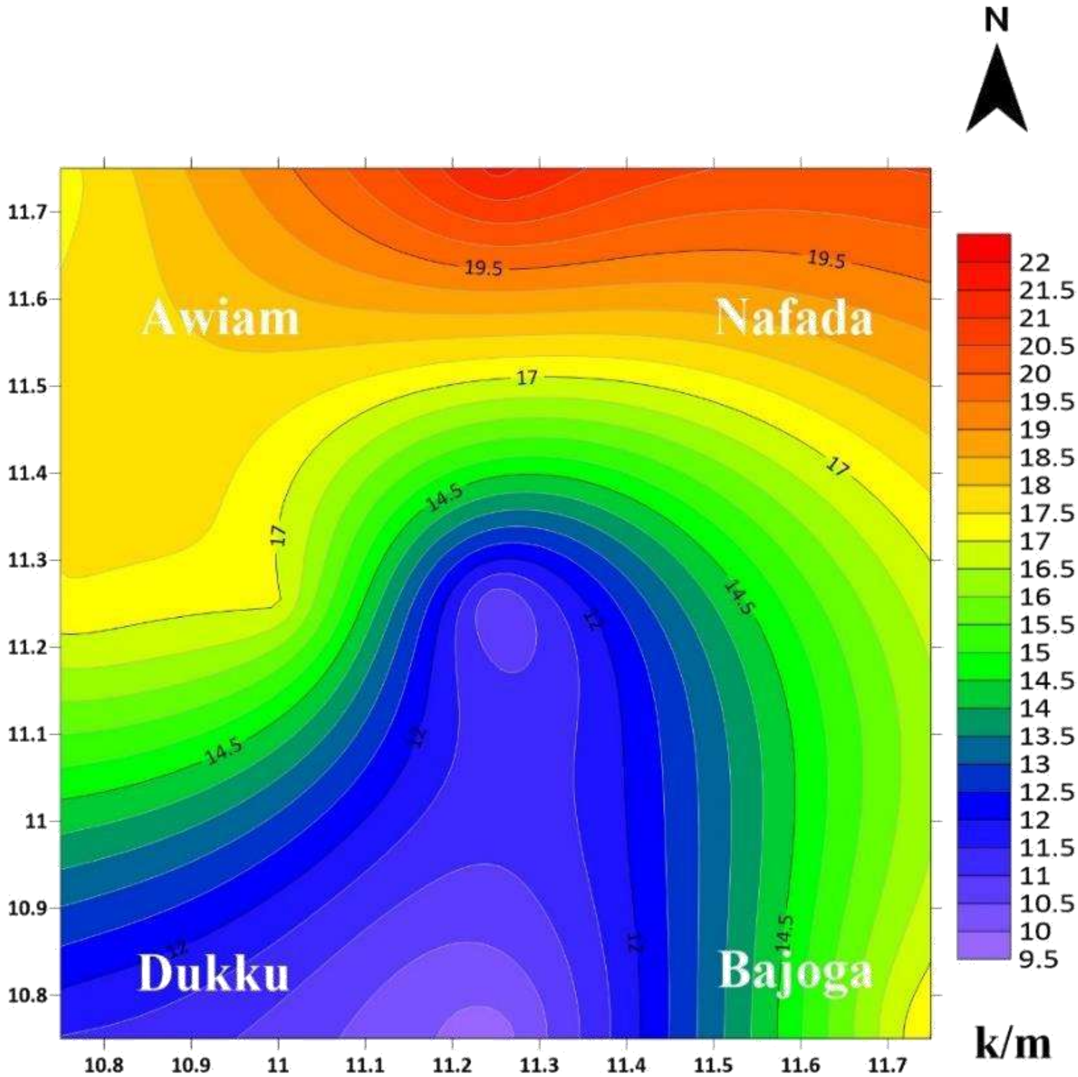

Figure 4.7: Contour map of the Curie point depth (Contour interval is 0.5 km)

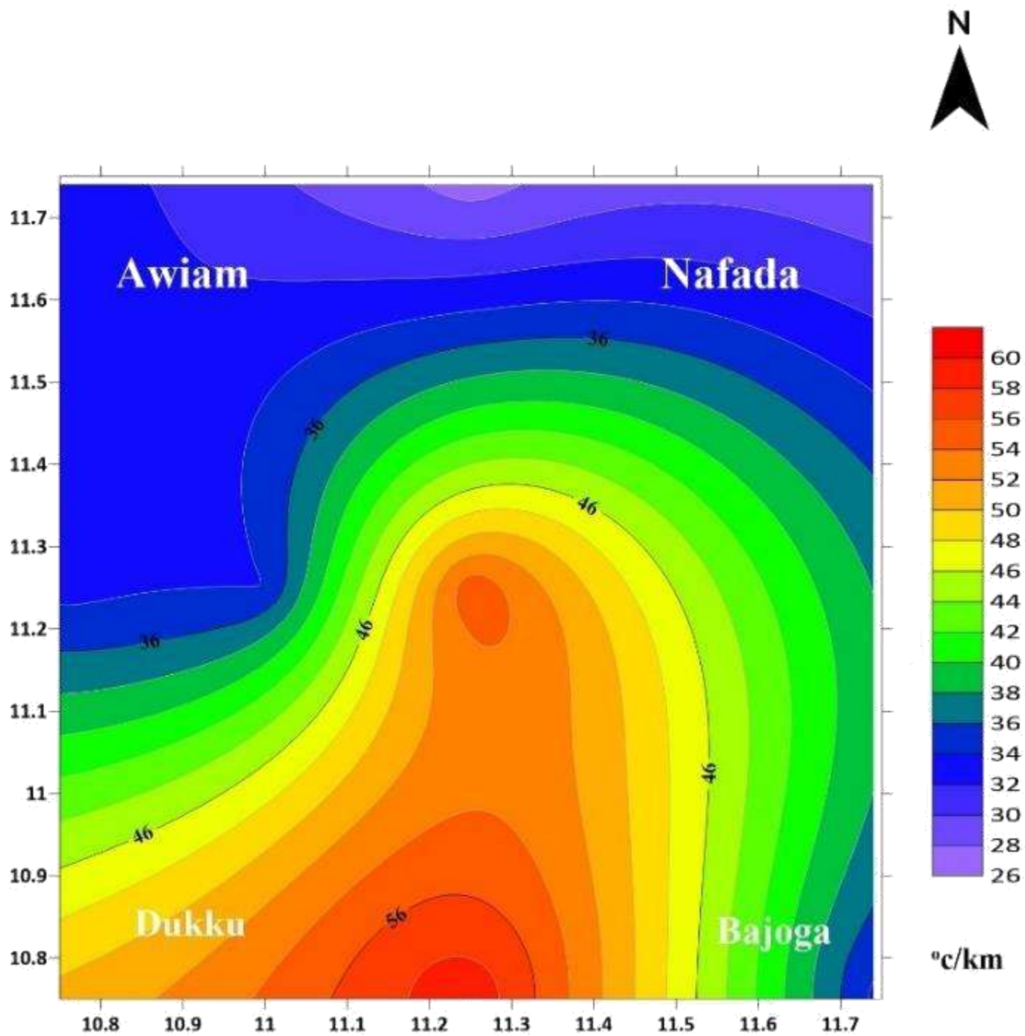

Figure 4.8: Contour map of the geothermal gradient (Contour interval 0.5 Ckm^{-1})

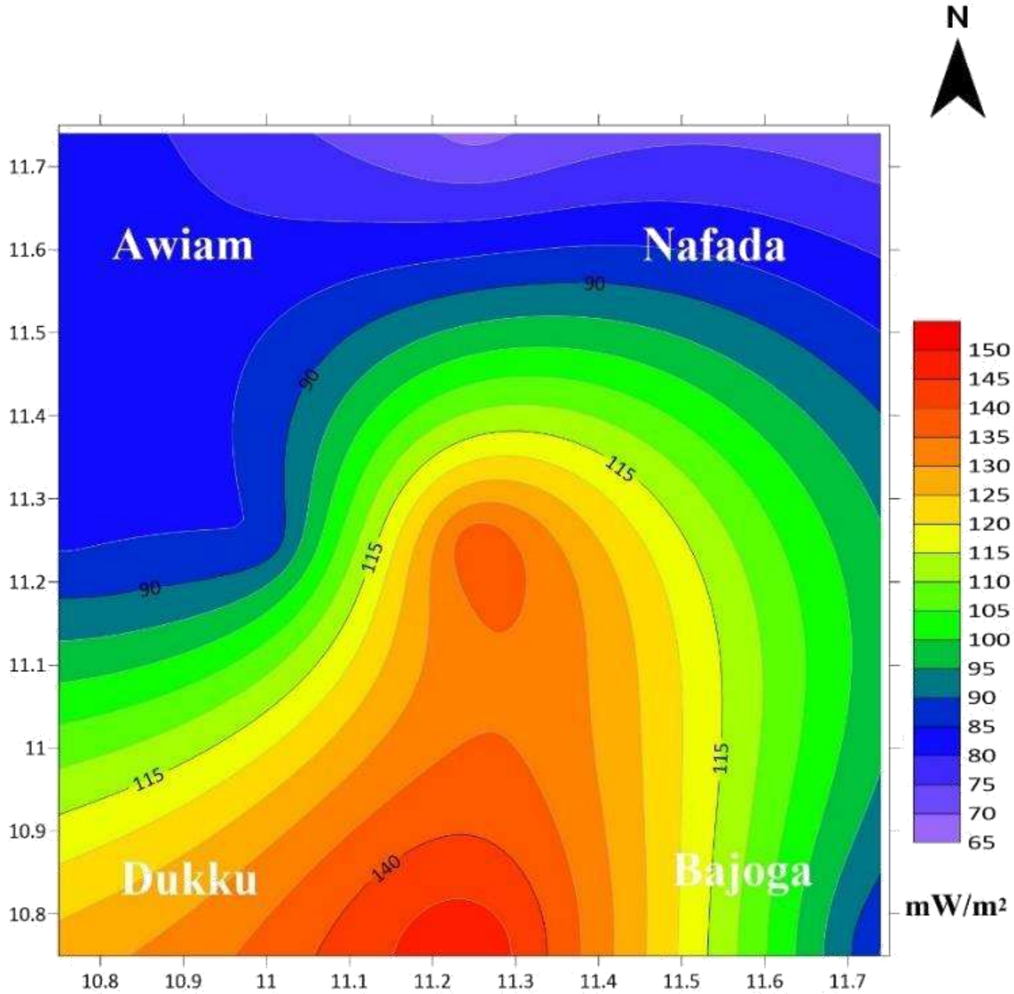

Figure 4.9: Contour map of the Heat flow anomaly (Contour interval of 5 mW/m^2)

4.2.2 Source parameter imaging (SP1) of the study area

The SPI map (Figure 4.11) obtained reveals two categories of depth sources; shallow source and deeper source. The area with blue colouration depicts the deeper source while the area with red colouration is for shallow sources. The shallow source is 0.17 km and deeper source is 4.2 km.

The area where the highest sedimentary thickness occur also conforms to the area of low amplitude magnetic values on both maps, which shows good similarity of the SP1 map with the analytic signal map of the study area.

The regions of shallow (pink colouration) and deeper (blue colouration) depth sources from the map (Figure 4.11) also conforms with the regions of high and low depths of depths to the top of the boundary (Z_t) obtained from spectral analysis. The low depth in the Northwestern part of the SPI also agrees with high amplitude anomalies in (Figure 4.4).

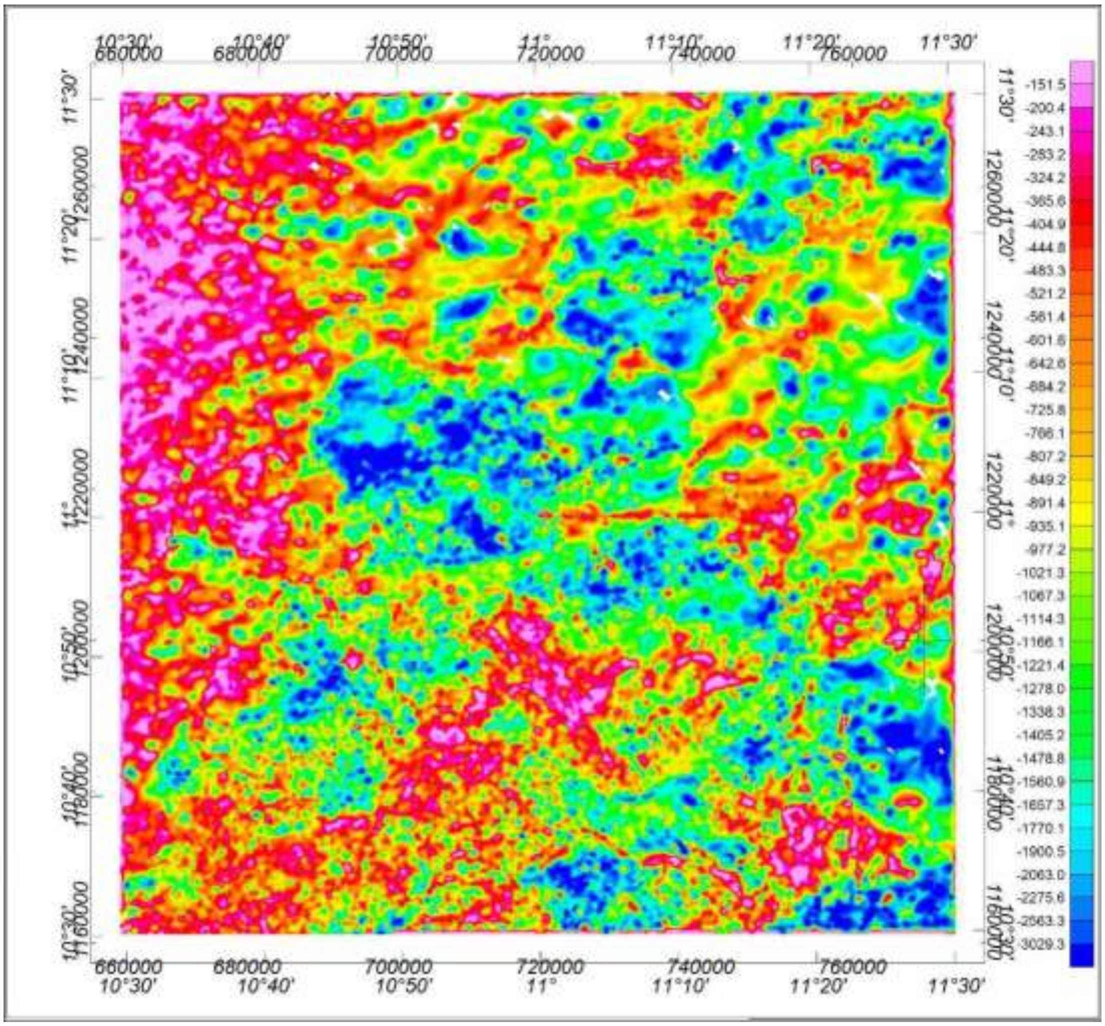

Figure 4.10: Source Parameter Imaging (SPI) of the study area

4.3 Radiogenic Heat Analysis

According to Megwara *et al.* (2013), Holmberg *et al.* (2012) and Abraham *et al.* (2014) radiogenic heat production (H) is primarily concerned with the decaying of radioactive isotopes of ^{232}Th, ^{238}U and ^{40}K and can be computed in accordance With the concentration (C) of the respective elements via the expression:

$$H(\mu W/m^3) = p(9.52\ C_u + 2.56\ C_{Th} + 3.48\ C_k)10^{-2} \qquad (4.1)$$

where,

H = radiogenic heat production

p = density of rock adapted from Telford *et al* (1990).

C_u, C_{Th} and C_k are the concentrations of Uranium, Thorium and Potassium respectively.

The concentration of the three radiometric elements were read from the radiometric map covering the study area with high geothermal gradient.

Therefore, from the above equation 4.1, at a maximum C_u = 10.2 ppm, C_{Th} = 31.0 ppm and C_k = 5.7 ppm.

4.3.1 Potassium (K) content map of the study area

The potassium (K) concentration map (Figure 4.12) of the study area shows high concentration of potassium observed at the eastern part and some portion of the northwestern part.

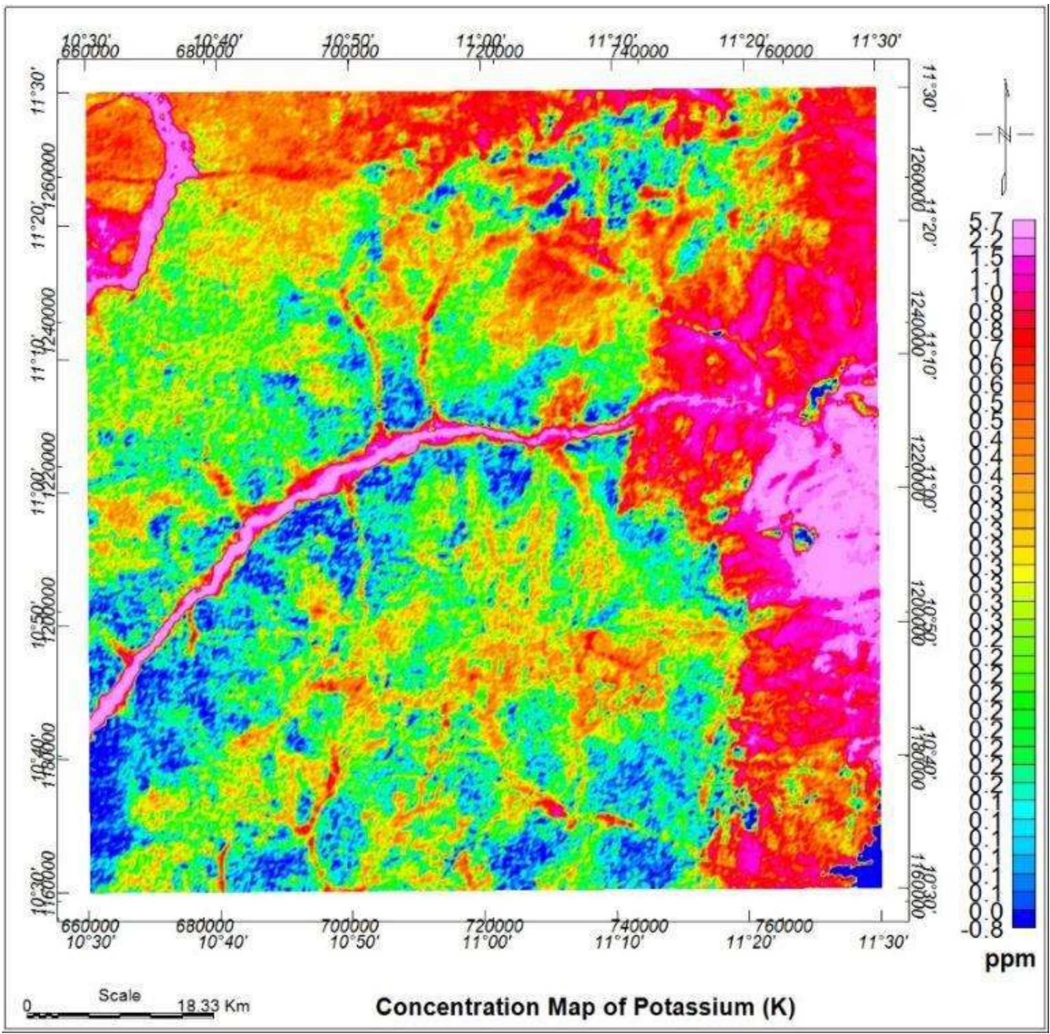

Figure 4.11: Concentration map of potassium (K) for the study area

Higher potassium concentrations is in the eastern part and some portion of the northwestern region corresponding to the area around Nafada and Bajoga. Mostly prevailing concentrations values of between 1.10 ppm and 5.70 ppm and it shows low concentration value in the region around Dukku and small portion of Bajoga. This low values may be associated with limestone, sandstone carbonaceous shales in the area.

It shows an inverse relationship with Figure. 4.9 (contour map of the geothermal gradient) and Figure 4.10 (contour map of the heat flow anomaly) as it shows low concentration value in a region with higher heat flow and low value in a region with low geothermal heat flow which may mean that K is not a contributor for the high heat flow in those area.

4.3.2 Thorium (Th) content map of the study area

Thorium concentration map in Figure 4.13 shows values ranging -8.0 to 31.0 in the whole of the study area. High concentration of Thorium is in most part of the eastern and some portion of the norther area, the concentration were not evenly distributed. Higher concentration values of between 15.5 ppm to 31.0 ppm is in the northern (Nafada) and eastern-central (Bajoga). Small portion of north-western (Awiam) region were also dominated by the high observed concentration value. Low value were found in central and southern part of the study area and at the edge of south-eastem part.

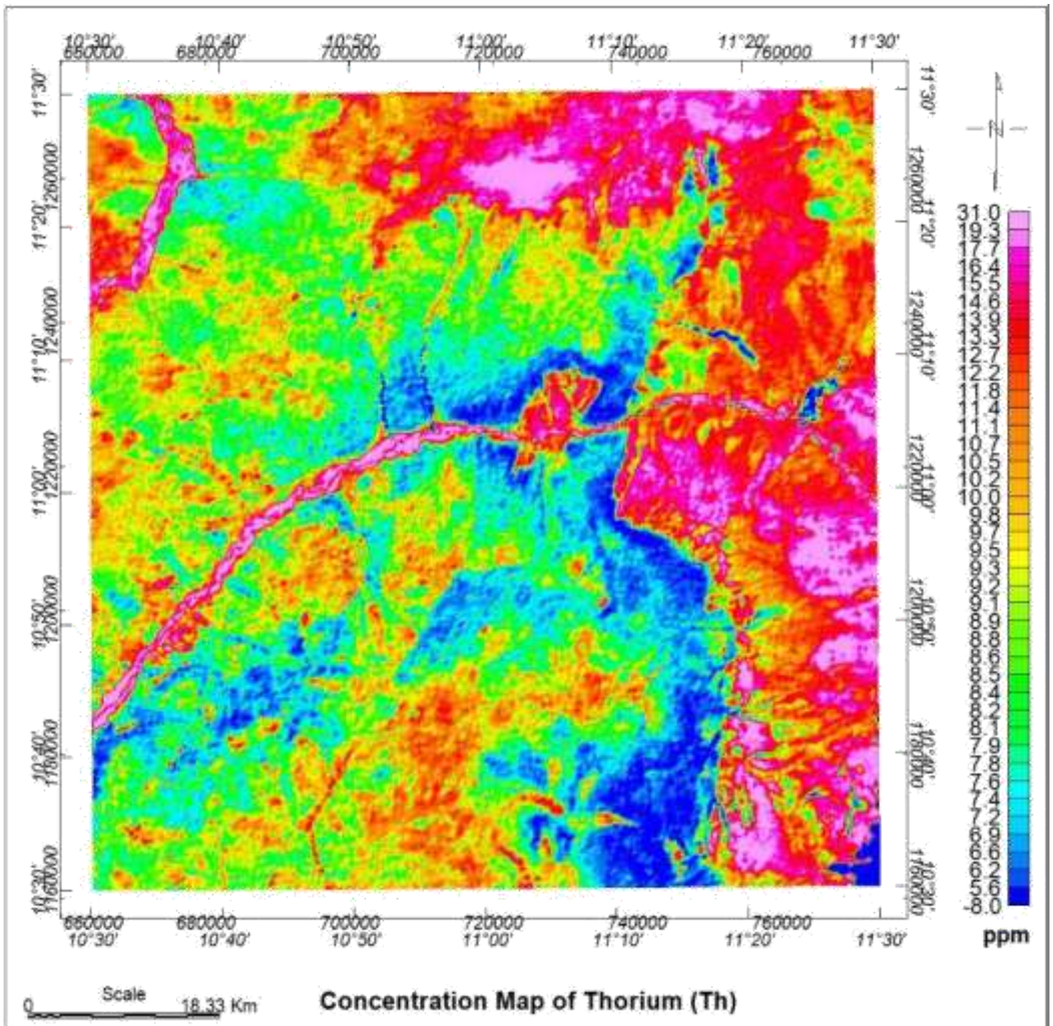

Figure 4.12: Concentration map of thorium (Th) for the study area

4.3.3 Uranium (U) content

The concentration map (figure 4.14) of uranium (U) shows high concentration of uranium (U) observed at the north, major part of eastern region, south-eastern and some portion of the north-western part. Also some trace of uranium (U) deposit can be observed at the riverine area trending from the east to west.

Low concentration of uranium (U) observed at small portion of south-eastern part, south-western and some part of the middle of study area.

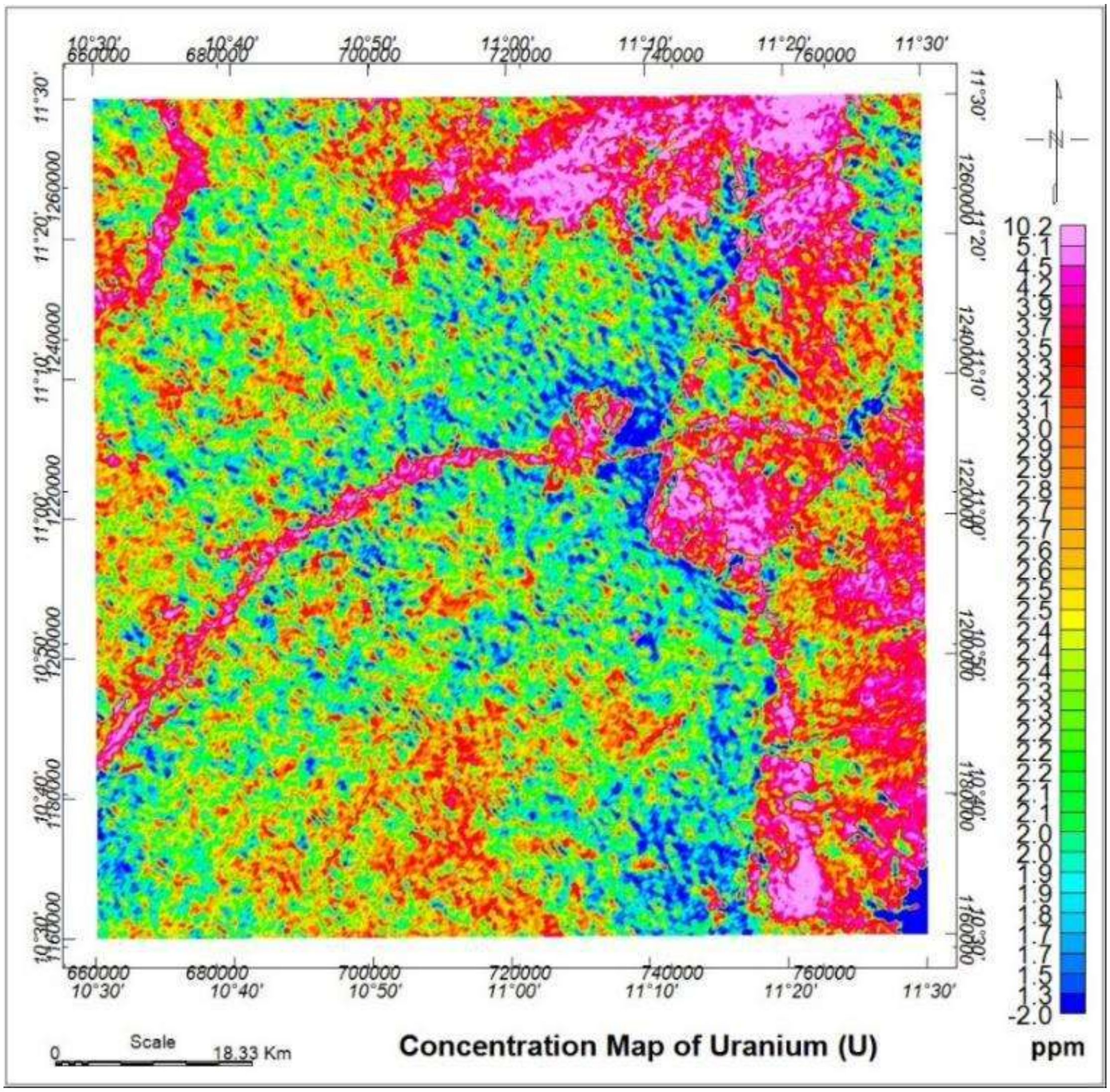

Figure 4.13: Concentration map of uranium (U) for the study area

4.3.4 Ternary map

The ternary map (Figure 4.14) of the area was generated from the combination of uranium, thorium and potassium concentrations, it depicts the concentration of K (in Red), Th (in green), and U (in blue), the white colour is related with high counts of the three isotopes, while the black colour depicts low levels of three isotopes.

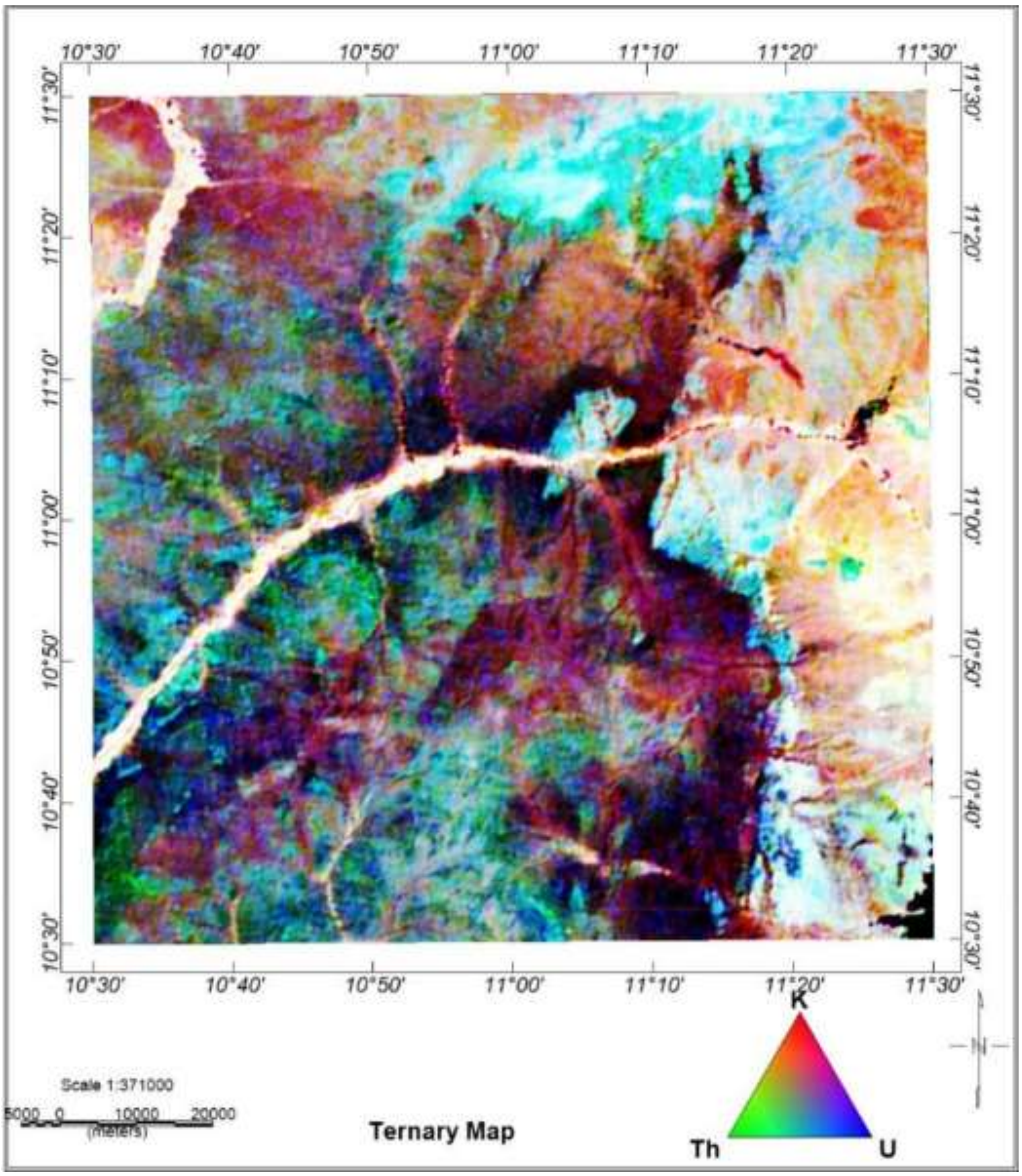

Figure 4.14: Ternary map of the study area

4.4 Radiogenic Heat Production (RHP)

The potassium, thorium and uranium content map of the study area were merge alongside with the Total Magnetic Intensity map. Ten profiles (Figure 4.15) drawn along the path with high heat flow (Figure 4.10), and average concentration of each isotope along each profile were computed.

Their average specific gravity or density alongside with average concentration of each isotope along each profile is further calculation on the radiogenic heat production. Radiogenic heat production (Table 4.2) values for each profile calculated based on Equation (3.25) with an average value of 1.43 $\mu W/m^3$.

From the result (Table 4.2), it shows that the average radioactive heat production obtained in profile 2 and 8 which majorly runs through region with high magnetic signatures (figure 4.1). Low heat flow (figure 4.10) while profile 7 and 10 that runs through region with low magnetic signatures (figure 4.1) and high heat flow (figure 4.10) has the highest values.

Table 4.2. Summary of the result for radiometric heat analysis

Isotopes	C_U (ppm)	C_{TH} (ppm)	C_K (ppm)	Total Count	RHP ($\mu W/m^3$)
PROFILE 1	2.7	10.1	0.4	13.2	1.43
PROFILE 2	2.4	8.9	0.3	11.6	1.26
PROFILE 3	2.5	9.4	0.3	12.2	1.32
PROFILE 4	2.5	9.9	0.3	12.8	1.35
PROFILE 5	2.6	9.9	0.3	12.8	1.38
PROFILE 6	2.6	9.5	0.3	12.4	1.35
PROFILE 7	3.8	14.2	0.8	18.8	2.03
PROFILE 8	2.4	8.8	0.3	11.5	1.25
PROFILE 9	2.5	9.2	0.3	12	1.31
PROFILE 10	2.8	11.4	0.7	14.9	1.57

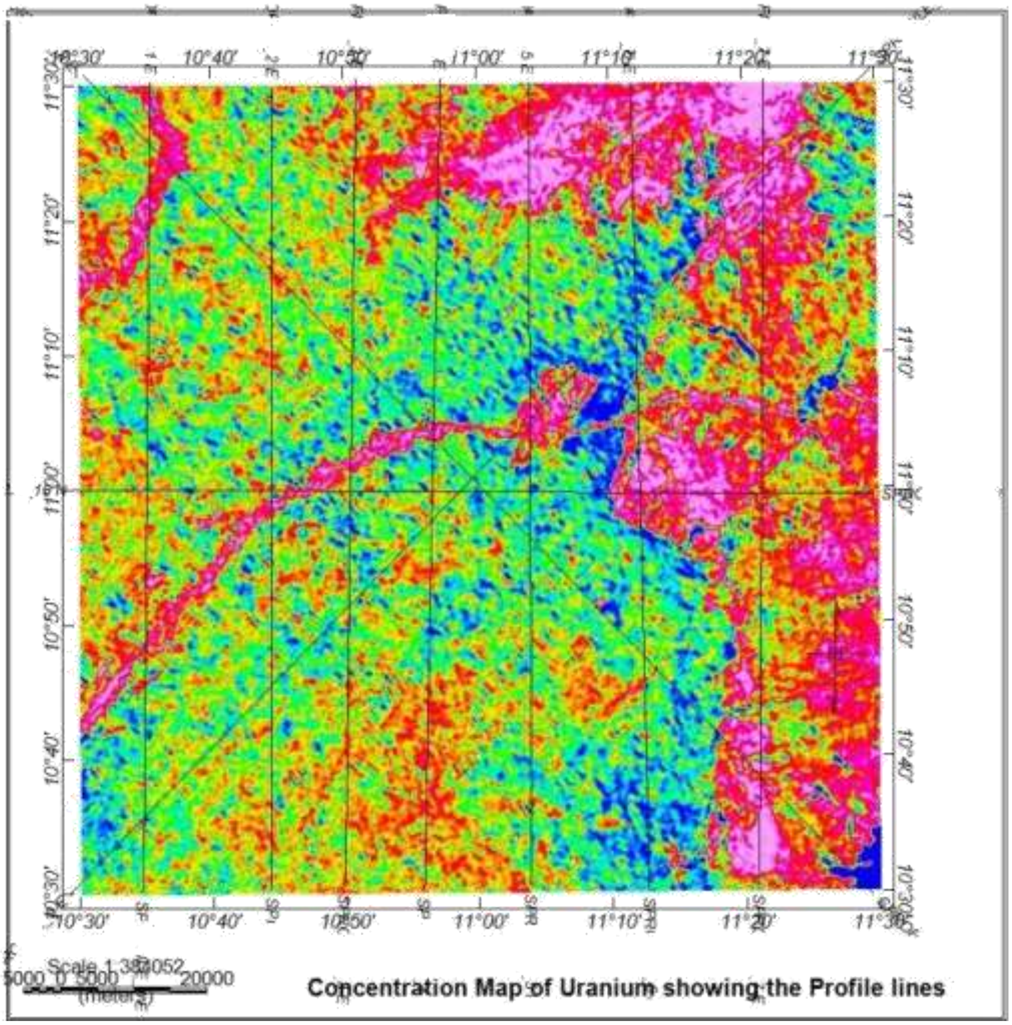

Figure 4.15: Map showing profiles where RHP were calculated

CHAPTER FIVE

5.0 CONCLUSION AND RECOMMENDATION

5.1 Conclusion

Qualitative interpretation has been performed on the Total magnetic intensity, regional, residual map anomaly and all this have explicitly distinguished the region of high magnetic properties from areas of low magnetic properties within the study area. Spectral analytical method was applied to estimate the sedimentary thickness and the centroid depth, for quality assurance of the spectral analytical method result both analytical signal map, source parameter imaging map were generated, and the three results were in conformity.

The difference in frequency characteristics between the magnetic effects from the bottom (centroid) and top boundary of the magnetised layer in the crust was used to estimate the depth to centroid, depth to top basement and Curie point in the study layer in line with equation 3.19, 3.20, 3.21, and 3.23. The Curie point depth in the study area ranges from 9.74 to 21.68 km with an average of 15.71 km.

The value varies between 9.5 km and 12.5 km in the southern part towards the central part of the study area (Dukku and Bajoga) dipping towards the southern and central, in the northern part of the study area. The values range between 19.5 km and 21.5 km increasing towards the central part. By contrast, higher values are located at the central (Awiam and Nafada). The Curie point depth results compared favourably with the result of Kasidi and Nur (2013).

Geothermal gradient, which is the rate of increase in temperature per unit depth, is a good indicator of sub-surface temperature distribution and is significant in the assessment of geothermal energy resources of an area. From the result (Table 4.1) the geothermal gradient, vary between 26.75 ^{o}C/km and 59.55 ^{o}C/km. The results (Table 4.1) shows that the heat flow values of the study area varies between 71.09 mW/m^2 and 150.07 mW/m^2, low values of 65 mW/m^2 to 90 mW/m^2 are located at the Northeastern and Northwestern part of area (Awiam and Bajoga) and higher value of 100 mW/m^2 to 150 mW/m^2 can be located at most part of the southcentral part (Dukku and Bajoga) this high value might be as a result of igneous intrusion or the dominance sandstone and limestone in the area. Both Geothermal gradient and heat flow shows a linear relationship in their lineament (both in locations and trend) as areas of high heat flow correspond to high geothermal gradient and also low heat correspond to low geothermal gradient respectively, both also' shows an inverse relationship to Curie point depth as projected by equation 3.23 and 3.24.

Analysis of uranium, thorium and potassium content map were performed to determine their variation or distribution in the study area. It shows that there is high concentration of Uranium and Thorium in Northeast and southeastern part which is not in correlation with the areas of high heat flow and geothermal gradient. It therefore means the result of radiometric heat production in the study area cannot be used to corroborate the results of the aeromagnetic data in that area. The average heat flow in thermally normal continental region is reported to be about 60 mW/m^2.

However, values between 80 mW/m^2 and 100 mW/m^2 are considered to be good geothermal reservoir and values above 100 mW/m2 is an indication of anomalous geothermal condition (Jessop *et al.,* 1976; Nwanko *et al.,* 2011; Suleiman *et al.,* 2020). In view of this, the estimated heat flow value of 80 mW/m^2 and above obtained around Awiam, Dukku (north/western), and Nafada and Bajoga (Northeastern and southeastern) region of the study area makes the area to be of favourable geothermal potentials.

The calculations of RHP (Table 4.2) based on equation 4.1 in the study area shows an average value of 1.43 $\mu W/m^3$. This value appears to be slightly greater than the average heat production of the Precambrian shield, 0.77 ± 0.08 $\mu W/m^3$ given by Jaupart *et al.*, (2003), although they indicated that on a local scale, the variation from their value could be significant. In the present study, the slight difference in the area RHP is attributed to the high radioelement contents.

5.2 Recommendations

The study has shown strong possibility of geothermal resource in the study area to explore for new and more energy locations in Nigeria. Therefore, the area is recommended for further investigation such as measurement of the area temperature at depth through a series of boreholes to be located at adequate intervals for an insight in to the geothermal gradient.

REFERENCES

Abdullahi. B. U., Rai, .1. K., Olaitan, O. M., & Musa Y. A. (2014). A review of the correlation between geology and geothermal energy in North-Eastem Nigeria. *Journal applied Geology and Geophysics* 1(2) 74-83.

Abraham, F. M., Lawa1, K.M., Ekwe, A.C., Alile, O., Murana, K. A., & Lawa1, A .A. (2014).Spectral analysis of aeromagnetic data for geothermal energy investigation of lkogosi Warm Spring-Ekiti State, southwestern Nigeria. *Geothermal Energy*, 2, 1-7.

Adighije, C. (l979). Gravity field of Benue Trough, *Nigeria, Nature Physical Science,* 282, 199201.

Ajakaiye, D. E. (1981). Geophysical investigations in the Benue trough-a review. *Earth Evolution Sciences* 2, 110-125.

Akande, S. O., Egenhoff, S. O., Obaje, N. G. & Erdtmann, B. D. (2011). Stratigraphic evolution and petroleum potential of middle cretaceous sediments in the lower and middle Benue Trough, Nigeri: insights from new source rock facies evaluation. *Petroleum Technology Development Journal* 72, 1128-1142

Ananaba, S. E., Ajakaiye, D.E. (1987). Evidence of Tectonic Control of mineralization in Nigeria from lineament density analysis A Landsat-study. *International Journal of Remote Sensing,* 8 (10), 1445 – 1453.

Aydin I., & Oksum E. (2010). Exponential Approach to Estimate the Curie-temperature depth. Journal of Geophysics and Engineering 7 (2) 113 – 125.

Bako A. S. J. (2010). Geothermal energy potential in the part of middle benue trough located in Nasarawa state. *A thesis submitted to the postgraduate school,* Ahmadu Bello University, Zaria, Nigeria.

Burke, K. D., & Whiteman, A.J. (1972). Geological history of the Benue valley and adjacent areas. In T.F.J. Dessauvagie and AJ. Whiteman (eds). African Geology; *University of Ibadan Press, Nigeria*, 187-206

Burke, K. C., Dessauvaagie, T.F.J. & Whiteman, A.J., (1972): *Geological History of the Benue Valley and Adjacent Areas.* In African Geology (Edited by Dessauvagie T.F.J and Whiteman A.J) eds. *Ibadan University press, Ibadan*. 187-205.

Duval J. S. (1983). Composite color images of aerial gamma-ray spectrometric data. Geophysics,

Eleta B. E., & Udensi E. E. (2012). Investigation of the Curie point isothermal from the magnetic field of easter section of Central Nigeria. *Geoscience* 2 (4) 101 - 106

Genik G. J. (1992). Regional framework structure and petroleum aspects of rift basins in Niger, Chad and Central African Republic. *Tectonophysics* 213 (1 - 2).

Grant, F. S. & West, G. (1965) Interpretation theory in applied geophysics. Fox. Publication, New York, NY McGraw-Hill. (2) 581- 584

Gupta S. K., Rajeev M. R., Sreekantan B. V., Srivatsan R., Tonwar S. C. (1991). Evidence for pulsed emission from the Crab pulsar at PeV energies. *Astronomy and Astrophysics*, 245 (1), 141 − 144.

Holmberg H., Naess E., & Evensen J.E. (2012) Thermal Modeling in the Oslo rift. In: ' *Norway. Proceedings, 37th workshop on geothermal reservoir engineering, Stanford University*

Jessop A. M. (1976) Geothermal energy from sedimentary basins. *United State Department of Energy Office of Scientific and Technical Information.* NP. 22308. EDB-77-131177

Kasidi, S. & Nur, A. (2013). Estimation of Curie point Depth, Heat Flow and Geothermal Gradient Inferred from Aeromagnetic Data over Jaligo and Environs. *International Journal of Science and Emerging Technology, 6(6), 294-301.*

Kearey, P, Brooks, M, & Hill, I. (2002), An Introduction to geophysical Exploration third Edition. *Blackwell Publishing*, ISBN 978 (0), 632

Khojamli, A., Avdejani, F. D., Moradzadah, A. & Kalate A. N. (2016). Estimation of Curie point depths and heat flow from Ardebil Province, Iran, Using Aeromagnetic data. *Arabian Journal of Geosciences.* 9 (5), 383 - 387.

Kurowska E. & Schoeneich, K. (2010). Geothermal Exploration in Nigeria. *Proceedings World Geothermal Congress Bali, Indonesia.* 25-29

Livia N., (2017). Borexino's search for low-energy neutrino and antineutrino signals correlated with gamma-ray bursts, *Astrophysics*, 86, 11 − 17.

Megwara J. U. & Udensi E. E. (2013) Lineaments study using aeromagnetic data over parts of southern Bida basin, Nigeria and the surrounding basement rocks. *International Journal of Basic and Applied Sciences* 2 (1) 115 - 119.

Megwara J. U., Udensi E. E. (2014). Structural analysis using aeromagnetic data: Case study of parts of southern Bida basin, Nigeria and the Surrounding basement rocks. *Earth science research* 3 (2) 27 - 36.

Muhammed S. B., Mustapha T. S. (2014). Analysis of Aeromagnetic data across Kebbi State, Nigeria. *International Journal of Atmospheric and Earth Sciences 2* (1) 41 – 51.

Murthy B.S.R 2007, Airborne Geophysics and the Indian Scenario. Geophysics Union, 11(1), 1–28.

Nabighian, MN. (1972). The analytic signal of two-dimensional magnetic bodies with polygonal cross-sections: Its properties and use for automated anomaly interpretation. *Geophysics*, 37, 507-517.

Nabighian, MN. (1984). Towards a three dimensional automatic interpretation of potential field data via generalized Hilbert transform fundamental relations. *Geophysics*. 47, 780-786.

Negi, J.G., Agrawal, P. K., & Rao, K.N.N. (1983). Three-dimensional model of the Koyan area of Maharshaitra state (India) based on the spectral analysis of aeromagnetic data. *Geophysics,* 48 (7), 964-974.

Nwankwo, L.I., Olasehinde, P.I., & Akoshile, CO. (2011). Heat 110w anomalies from the spectral analysis of airborne magnetic data of Nupe Basin, Nigeria. *Asian Journal of Earth Sciences*, 1(1), 1-6

Nwogbo P. O. (1997). Mapping the shallow magnetic sources in the upper Benue basin of Nigeria from Aeromagneitc Spectra. Africa Geoscience Review 4, 325 – 334.

Nwosu O. B. (2014). Determination of magnetic basement depth over part of middle Benue Trough by Source Parameter Imaging (SPI) technique using High Aeromagnetic Map. International Journal of Science 31, 1 – 10.

Obaje, N. G., Funtua, I.I., Ligouis, B., and Abaa, S.I. (1998). Organic Maturation and Coal-Derived Hydrocarbon Potentials of Cretaceous Coal Measures in the Middle Benue Trough of Nigeria. *Journal of Mining and Geology*. 34: No 1, 7-18.

Obaje, N.G. (2009). Geology and mineral resources of Nigeria. Springer, Dordrecht Heidelberg London New York, 221

Obande E. Kolawole M. L., & Lawal A. A., (2014) Corrigendum to Spectral analysis of aeromagnetic data for geothermal investigation of Wikki Warm Spring, north-east Nigeria. *Geothermics 50 (2014) 85–90*

Ofoegbu, C.O., &Onuoha, KM. (1991). Analysis of magnetic data over the Abakaliki anticlinorium of the lower Benue trough Nigeria. *Marine and Petroleum Geology,* 8, 174-183.

Okwesili N., Okeke F. N., & Orji P. O. (2021). Geophysical survey of aerogravity anomalies over Lafia and Akiri regions of middle Benue trough, Nigeria, employing Power Spectrum and Source Parameter Imaging technique. IOSR Journal of Applied Physics 12(05):2278-4861

Onuoha, K. M., Ofoegbu, C. O., Ahmed M.N. (1994).Spectral analysis of aeromagnetic data over the middle Benue Trough, Nigeria. *Journal of Mining and Geology,* 30(2), 21 1-217.

Osazua, l. B., Ajakaiye, D. E., &Verheiien, P. J. T. (1981). Analysis of the structure of part of the upper Benue rift valley on the basis of new geophysical data. *Earth Evolution Sciences* 2, 126-135.

Petters, S.W. (1977). Mid Cretaceous Paleoenvironments and biostratigraphy of the Benue Trough, Nigeria: *Geological Society of America*, 89, 151-154.

Quijano, L., Gaspar L., & Lopez-Vicente M. (2011) Soil magnetic susceptibility and surface topographic characteristics in cultivated soils. *Latinmag letters,* 1(2), 1-6.

Roest, W.R., Verhoef, J., & Pilkington, M. (1992). Magnetic interpretation using the 3D analytic signal. Geophysics, 57, 116-125.

Rolandone F., Mareschal J. & Jaupart C. (2003) Temperatures at the base of the Laurentide Ice Sheet inferred from borehole temperature data. *Geophysical Research Letters. Vol. 30 (18)* 10.1029 GL018046

Salako, (2014). Depth to Basement Determination Using Source Parameter Imaging (SP1) of Aeromagnetic Data: An Application to Upper Benue Trough and Borno Basin, Northeast, Nigeria. *Academic Research International*, 74 -86.

Salako, K. A., Udensi, E. E (2013). Spectral depth analysis of parts of upper BenueTrough and Borno Basin, North-East Nigeria, Using Aeromagnetic Data, *International Journal of Science and Research,* 2(8)48-55.

Sharma P. V. (1987). Magnetic method applied to mineral exploration. Ore Geology Reviews 2 (4) 323 – 357.

Shehu, A.T. Udensi, E.E. Adeniyi, J.O., & Jonah, SA. (2004). Spectral analysis of magnetic residual anomalies over the upper Sokoto Basin, Nigeria. *Zuma Journal of pure and Applied Science*, 6 (2), 37-49.

Slagstad T. (2008). Radiogenic heat production of Archean to Permian geological provinces in Norway. *Norsk Geologisk Tidsskrift*, 88(3), 149-166

Spector, A., & Grant, RS. (1970): Statistical models for interpreting aeromagnetic data. *Geophysics,* 35, 293-302.

Suleiman T., Okeke F. N. & Obiora N. D., (2020). Interpretation of aeromagnetic data over some parts of Sokoto Basin, Nigeria, using source parameter imaging and 3D Euler deconvolution methods. *International Journal of Physical Sciences.* Vol. 15(2), pp. 90-98, ISSN 1992-1950

Tanaka, A., Okubo, Y., & Matsubayashi, O. (1999). Curie point depth based on spectrum analysis of the magnetic anomaly data in East and Southeast Asia. *Tectonophysics,* 306, 461-470.

Telford, W.M., Geldart, L. P., & Sheriff, R. E. (1990). *Applied geophysics*. Cambridge University Press. 3, 85-86.

Tselentis, G.A. (1991). An attempt to define curie depth in Greece from aeromagnetic and heat flow data. *Pure and Applied Geophysics,* 136 (1), 87-101.

Thalén T. R. (1879). Spectral Analysis of New Earth. *Nature* 403.1905-08 24. ISSN 1476-4687 issue 24 August 1905

Udensi E. E. (2000). Interpretation of the total magnetic field over the Nupe basin in West Central Nigeria, using aeromagnetic data. *PhD thesis Ahmadu Bello University* Zaria Nigeria.

Udensi E. E. (2001). Two and half dimensional modeling of the sandstone thickness of the pategi area, central Nigeria, Using Aeromagnetic data. *Geological Society of Sweden*. 126, 93 – 98.

Udensi, E. E., & Osazuwa, I. B. (2003). Spectral determination of the depths to the buried magnetic rocks under the Nupe Basin, Nigeria. *Nigerian Journal of Physics*, 15(1), 51-59

LIST OF TABLES

APPENDICES

These appendixes contain other MATLAB plot of spectral energy against wavenumber.

Appendix A: Matlab plot of spectral energy against frequency for block 1

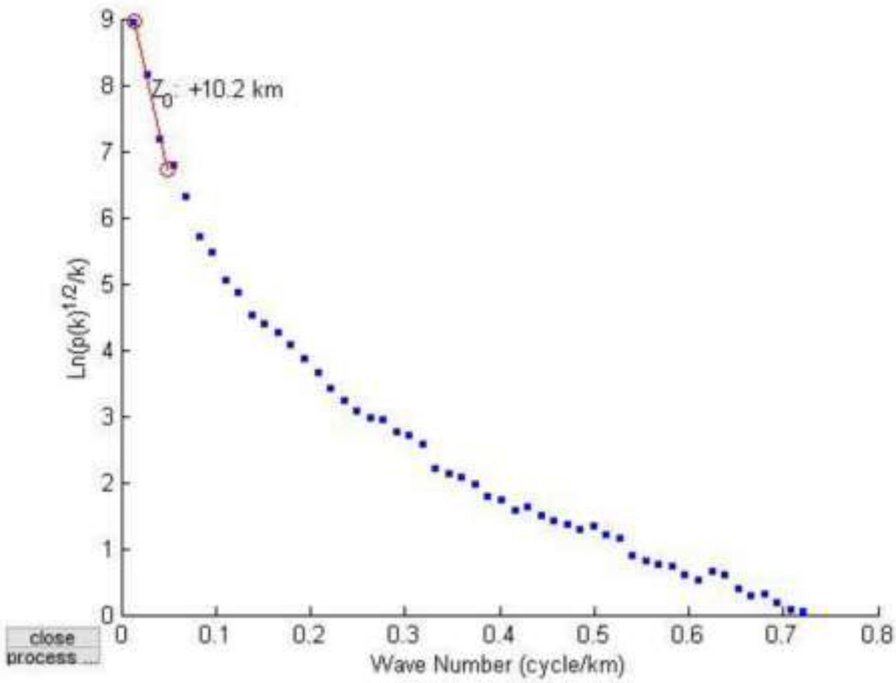

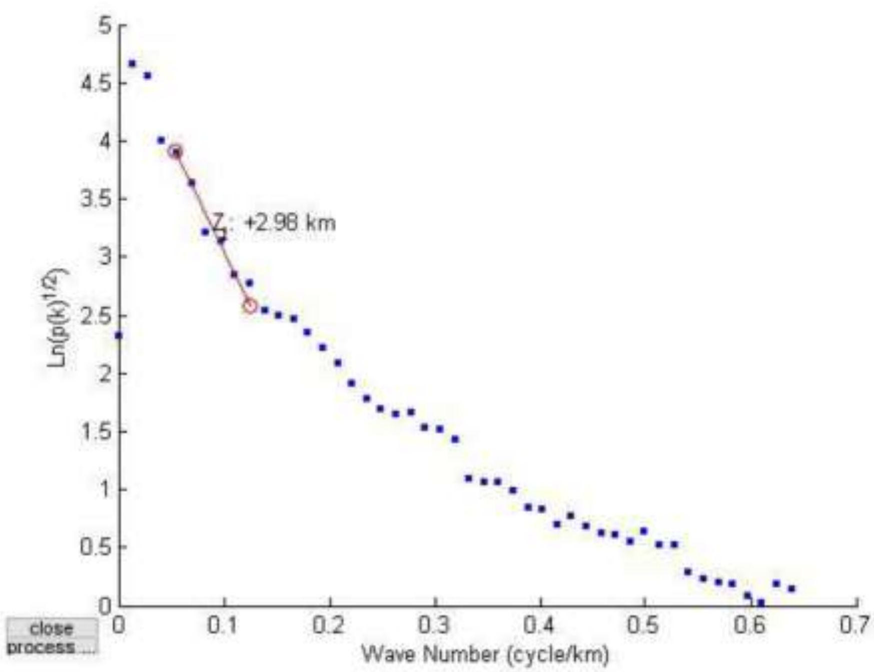

Appendix B: Matlab plot of spectral energy against frequency for block 2

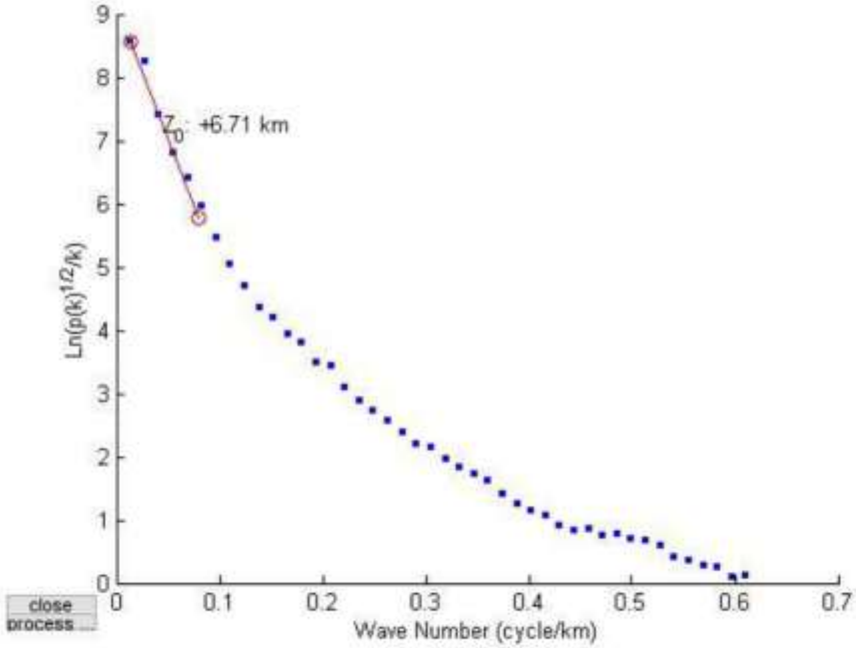

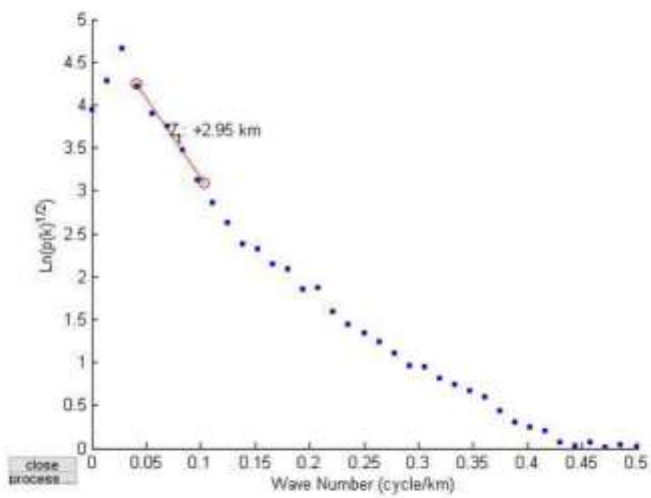

:

Appendix C: Matlab plot of spectral energy against frequency for block 3

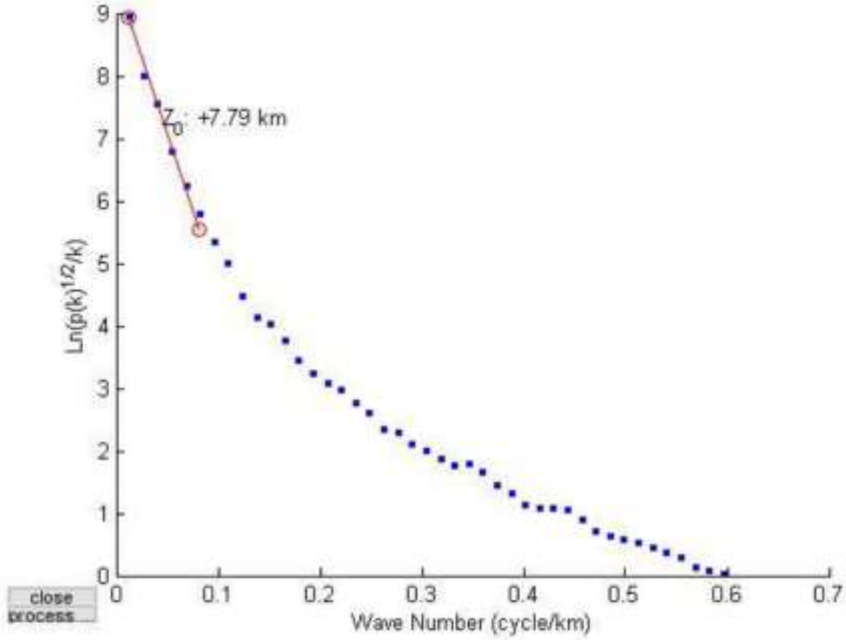

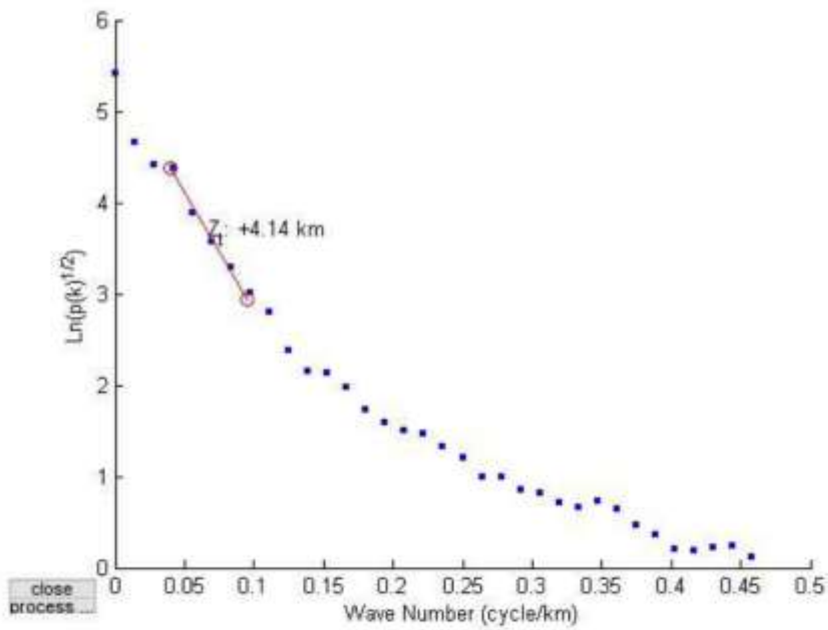

Appendix D: Matlab plot of spectral energy against frequency for block 4

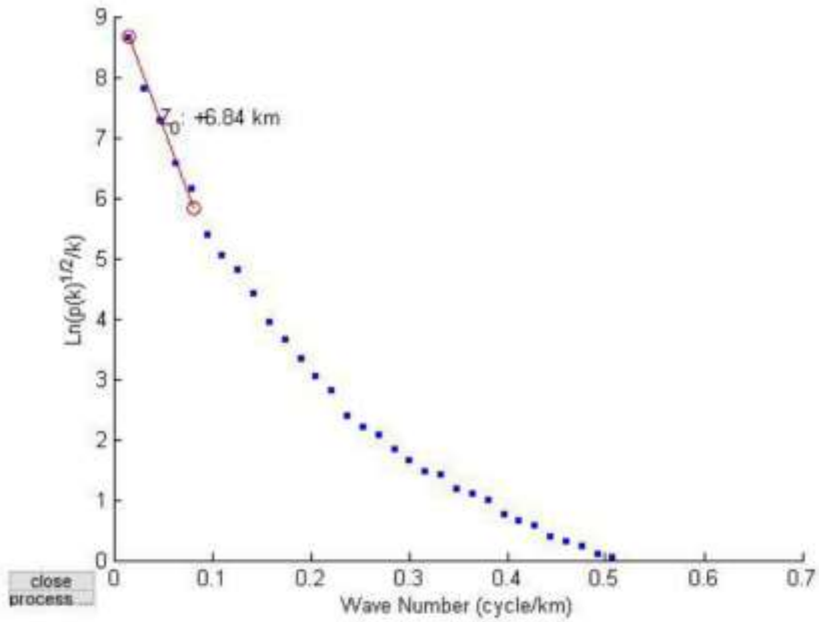

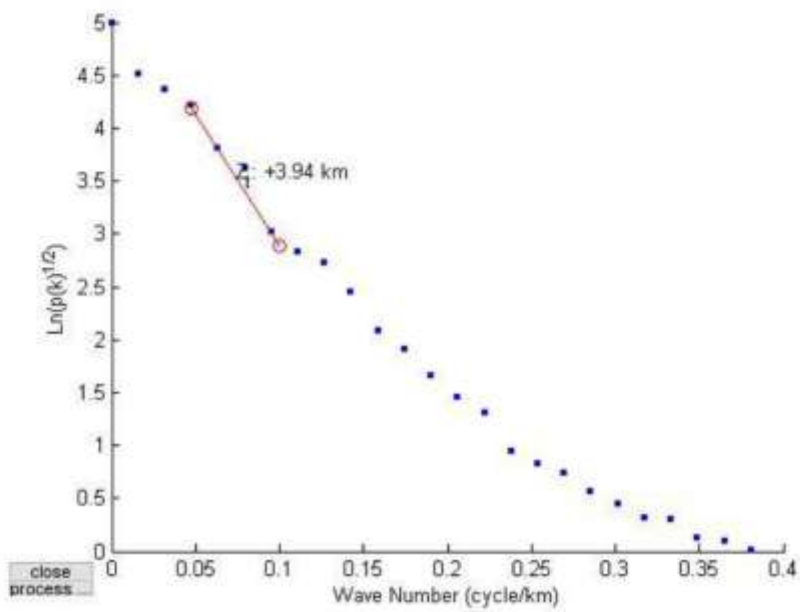

Appendix E: Matlab plot of spectral energy against frequency for block 5

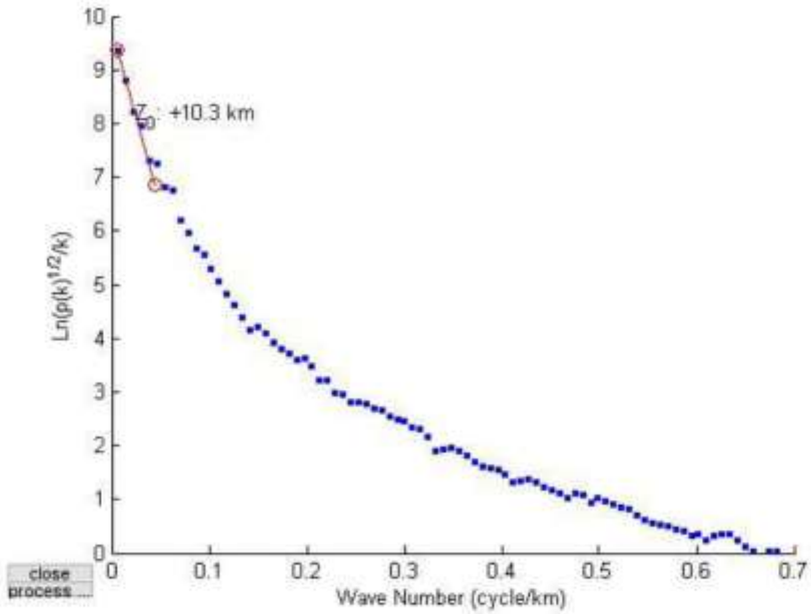

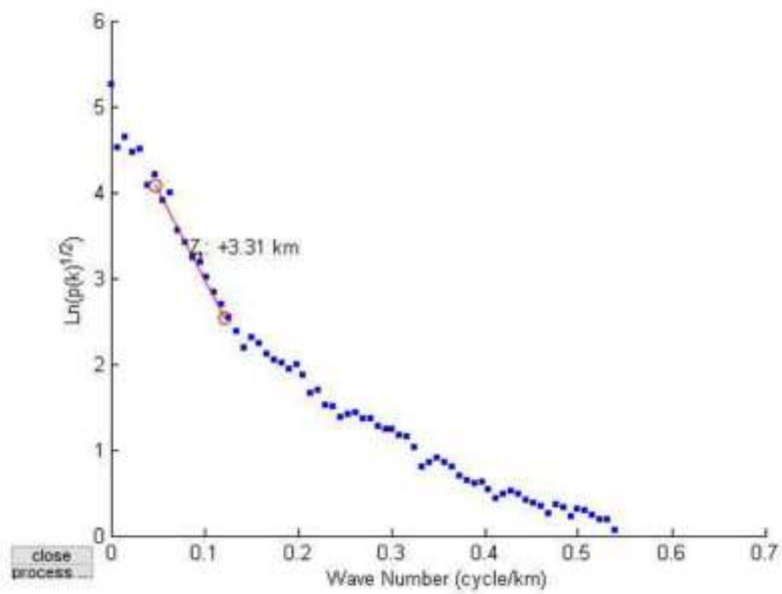

Appendix F: Matlab plot of spectral energy against frequency for block 6

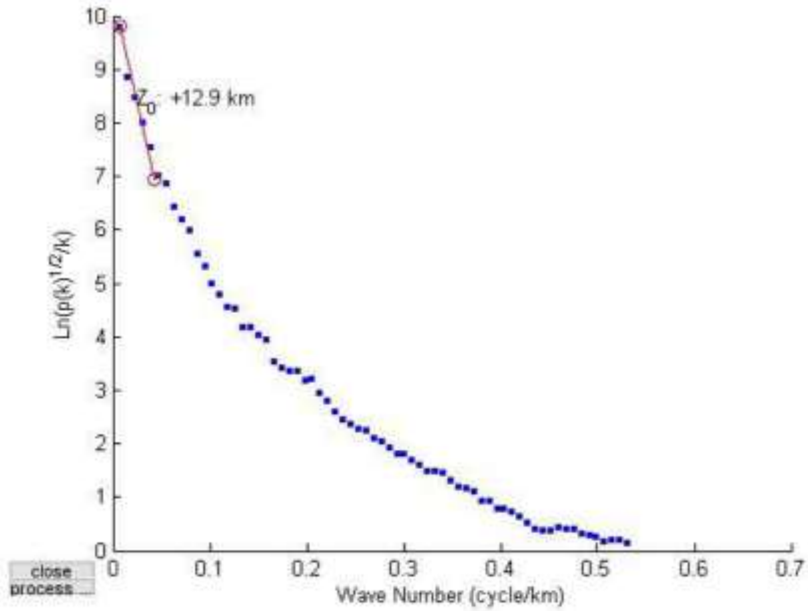

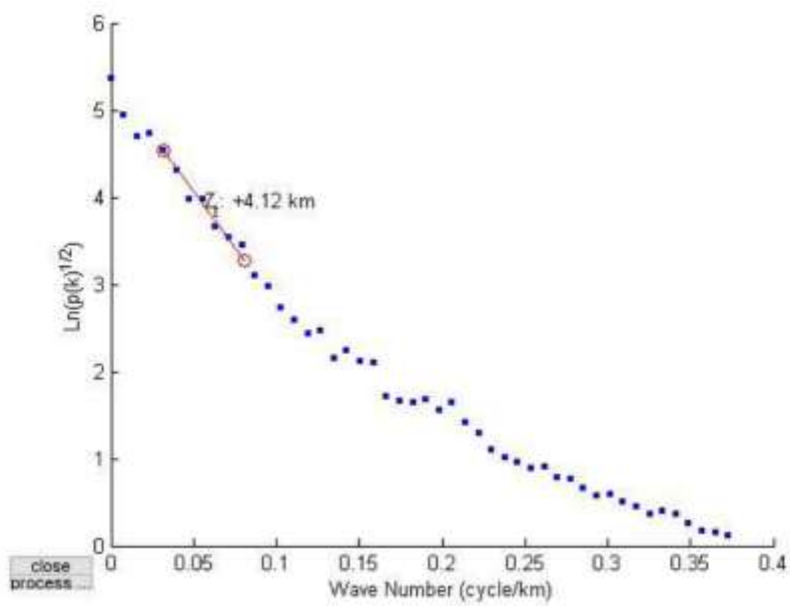

Appendix G: Matlab plot of spectral energy against frequency for block 7

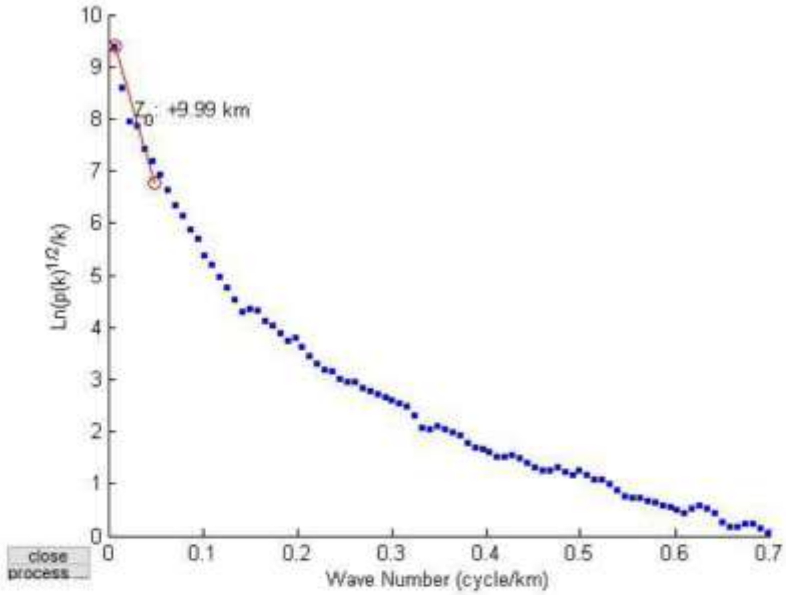

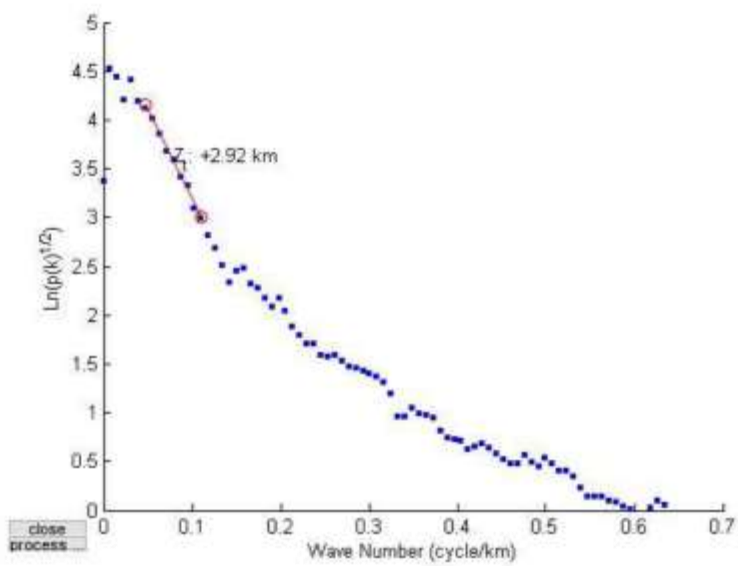

Appendix H: Matlab plot of spectral energy against frequency for block 8

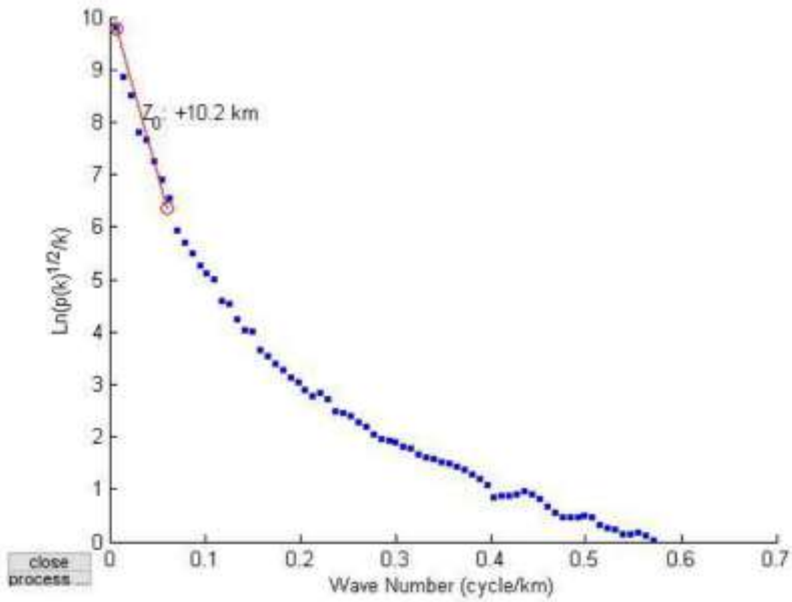

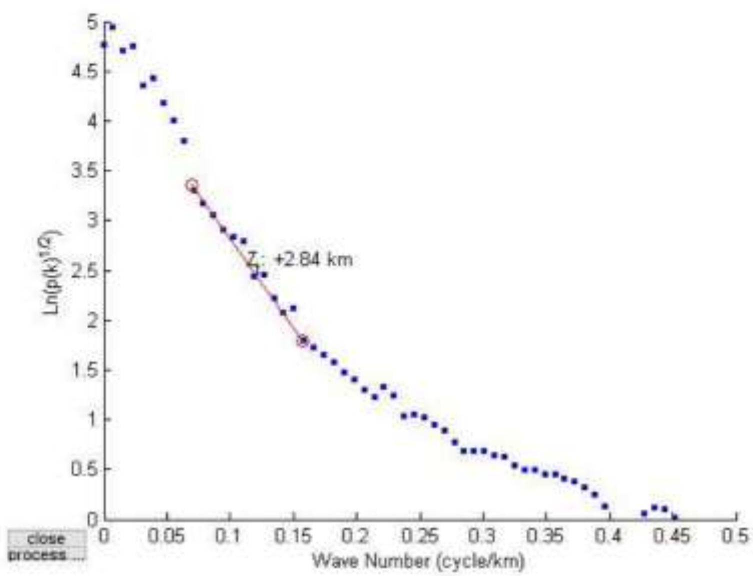

Appendix I: Matlab plot of spectral energy against frequency for block 9